First Principles Studies on Chemical and Electronic Structures of Adsorbates

Wenhua Zhang

Theoretical Chemistry
Royal Institute of Technology
Stockholm 2009

ISBN 978-91-7415-278-4
ISSN 1654-2312
TRITA-BIO Report 2009:8
Printed by Universitetsservice US-AB,
Stockholm, Sweden, 2009

To my family: past, future and present

Abstract

In this thesis, we focus on theoretical study of adsorbates on metal and oxide surfaces that are important for surface chemistry and catalysis. Based on first principles calculations, the adsorption of CO, NO, NO_2, $C_4H_6S_2$, $C_{22}H_{27}SH$ and other molecules or radicals on nobel metal surfaces (gold and silver) are investigated. Also, NO oxidation on oxygen pre-covered Au(111) surface and CO oxidation on water-oxygen covered Au(111)surface are theoretically studied. A new mechanism of water-enhanced CO oxidation is proposed. As for oxide surfaces, we first investigate the geometric, electronic and magnetic structures of FeO ultrathin film on Pt(111) surface. The experimentally observed scanning tunneling microscopy images are well reproduced for the first time with our model. The adsorption and dissociation of water on rutile TiO_2(110) surface are investigated by quantum molecular dynamics. By theoretical X-ray photoemission spectroscopy (XPS) calculations, the surface species are properly assigned. The same strategy has applied to the study of the phase transition of water covered reconstructed anatase TiO_2(001) surface, from which two different phases are theoretically identified. The structure of graphene oxide is also studied by comparing experimental and theoretical XPS spectra. Based on the novel structures identified, a new cut mechanism of graphene oxide is proposed.

Preface

The work presented in this thesis has been carried out at the Department of Theoretical Chemistry, School of Biotechnology, Royal Institute of Technology, Stockholm, Sweden and Istituto per i Processi Chimico-Fisici del Consiglio Nazionale delle Ricerche (IPCF-CNR), Pisa, Italy.

List of papers included in the thesis

Paper I A first-principles study of NO adsorption and oxidation on Au(111) surface
Wenhua Zhang, Zhenyu Li, Yi Luo and Jinlong Yang
J. Chem. Phys. **129**, 134708(2008).

Paper II Density Functional Study on the Mechanism of CO Oxidation with Activated Water on O/Au(111) Surface
Wenhua Zhang, Zhenyu Li, Yi Luo and Jinlong Yang
Chin. Sci. Bull. In press(2009).

Paper III Electron structure of [121] tetramantane-6-thiol on gold and silver surfaces
Wenhua Zhang, Bin Gao, Jinlong Yang, Ziyu Wu, Vicenzo Carravetta and Yi Luo
J. Chem. Phys. **130**, 054705(2009).

Paper IV First-Principles Study on Different BDT-gold Contact Structures
Wenhua Zhang, Vincenzo Carravetta, Jinlong Yang, and Yi Luo
In manuscript (2009).

Paper V First principles study of the geometric and electronic structure of FeO/Pt(111)
Wenhua Zhang, Zhenyu Li, Yi Luo and Jinlong Yang
J. Phys. Chem. C 00 (2009) 000.

Paper VI Quantum molecular dynamics study of water on TiO_2(110) surface
Wenhua Zhang, Jinlong Yang, Yi Luo, Susanna Monti, Vincenzo Carravetta
J. Chem. Phys. **129**, 064703(2008) .

Paper VII Interaction of biomolecular systems with titanium-based materials: computational investigations
Vincenzo Carravetta, Susanna Monti and Wenhua Zhang
Theor. Chem. Account In press (2009) .

Paper VIII Theoretical study on phase transition of water covered anatase TiO_2 (001) surface
Wenhua Zhang, Susanna Monti, Anders Sandell, Jinlong Yang, Vincenzo Carravetta and Yi Luo.
In manuscript(2009).

Paper IX Theoretical study of X-ray photoemission spectra of graphene oxides
Wenhua Zhang, Vincenzo Carravetta, Zhenyu Li, Yi Luo and Jinlong Yang.
In manuscript(2009).

Paper X How graphene is cut upon oxidation?
Zhenyu Li, Wenhua Zhang, Yi Luo, Jinlong Yang and Jianguo Hou
J. Am. Chem. Soc., Revision. (2009).

List of papers not included in the thesis

Paper I Photoinduced Formation of N_2 Molecules in Ammonium Compounds
E. F. Aziz, J. Grasjoe, J. Forsberg, E. Andersson, J. Soederstroem, L. Duda, W.-H. Zhang, J. L. Yang, S. Eise
J. Phys. Chem. A **111**, 9662(2007).

Paper II Effects due to inter-adsorbate interactions on the dipeptide/TiO_2 surface binding mechanism investigated by molecular dynamics simulations
Susanna Monti, Vincenzo Carravetta, Wenhua Zhang and Jinlong Yang
J. Phys. Chem. C **111**, 7765 (2007).

Paper III Electronic structure of aromatic amino acids studied by soft X-ray spectroscopy
Oksana Plekan, Vitaliy Feyer, Robert Richter, Marcello Coreno, Kevin C. Prince, Wenhua Zhang and Vincenzo Carravetta
In manuscript(2009).

Comments on my contribution to the papers included

- I was responsible for all the calculations and the writing of first drafts of **Paper I**, **Paper II**, **Paper IV**, **Paper V**, **Paper VI**, **Paper VIII** and **Paper IX** .

- I was responsible for part of the calculations (periodic part) and part of the writing of first draft of **Paper III**.

- I was responsible for part of the calculations for **Paper VII** and **Paper X**.

Acknowledgments

This thesis could not have reached its present form without the generous help of many people:

My deepest gratitude goes first and foremost to Prof. Yi Luo, my supervisor, for his constant encouragement and patience. He makes me realize that the supervisor could be a great friend who works with and helps you whenever it is needed. His optimistic attitude to work as well as ordinary life impresses me a lot. He has given me many useful suggestions about how to work and how to live. Here, I also want to appreciate Luo's family: Dr. Kezhao Xing and two kids Linda and Oscar for the happy moments they have brought to me.

Enormous thanks and gratitude will be devoted to my supervisor Prof. Jinlong Yang at University of Science and Technology of China(USTC), who trusted me even if I lost my confidence and provided me the opportunity to study here in Stockholm. Without this trust, I do not know where I would be.

Also many thanks to Prof. Vincenzo Carravetta, my third supervisor, whose precise attitude to science deeply impresses me. Thanks for your advises, discussion and the great efforts you have made to revise my papers. With your help I published my first scientific paper. The collaboration with you opened a new research field for me. You make me feel I am working with my supervisor, and also my friend. Great thanks to your care during the days I was in Pisa.

To be your three's student is the great fortune for my life. Great thanks to you.

There is another important person for making this thesis possible: Prof. Hans Ågren – the head of our department. I really appreciate you for giving me the opportunity to study at the Theoretical Chemistry group. Last but not least, thank you for leading such a nice and amazing group, I love our group beyond words.

I wish to thank all the present and former group members, it is you to make this group unique, to make my life here so nice. Many thanks to Prof. Boris Minaev, Prof. Faris Gel'mukhanov, Dr. Fahmi Himo, Dr. Paweł Sałek, Dr. Olav Vahtras, Dr. Yaoquan Tu and Dr. Zilvinas Rinkevicius for all your good lectures and helpful discussions. Thanks to our administrative staff, Pia and Lotta, for helping with many practical problems. Thanks to Bin Gao for the help of software and computer related problems.

There are some people who deserve certain attention: Na Lin and her handy husband Zhitai Jia. Thanks for Na Lin, the three years we have survived together

will be the best memory in the future days. Also thanks to my friends: Jun Jiang and his nice family DanDan and DouDou, Feng Zhang, Qiong Zhang, Bin Gao, Yanhua Wang, Ke Zhao, Dr. Tian-Tian Han (Dr. TT), Kai Liu, Guangde Tu, Yong Zeng, Shilu Chen, Kai Fu, Rongzhen Liao, Hui Cao, Jicai Liu, Ying Zhang, Keyan Lian, Sai Duan, Xiaofei Li, Kathrin, Elias, and many other friends in our group, I here express my thankfulness for all the happy time we shared.

I also wish to thank Prof. Zhenyu Li at USTC. Thanks for the best discussion with you and also the effort you have put in to my papers. Also thanks will be given to Prof. Weixin Huang and other collaborators for the great discussions and collaborations. I appreciate all the anonymous referees for your great comments and suggestions, from which I have learnt a lot.

Also thanks should be given to Prof. Antonio Rizzo for your help when I was in Pisa. Jing Huang and Jian Song are the best room-mates and friends of mine. Thanks to Hao Ren, Shuanglin Hu, Qiang Fu. Also thanks to all the members in Prof. Yang's group.

Finally, my special thanks go to my parents for their love and support. You made me what I am and I sincerely hope that I can pay you back in way or the other. Weihua Chen, my husband, thanks for taking me to your world and the future life we will share together.

Contents

1

Introduction

"Everything has its beauty but not everyone sees it."

Confucius, Analects, ca. 500 BC.

Surface science is a subject discipline to study the physical and chemical phenomena that occur at the interface of two phases, including liquid-gas, solid-gas, liquid-liquid, liquid-solid and solid-solid interfaces. It encompasses concepts such as heterogeneous catalysis, semiconductor device fabrication, fuel cells, self-assembled monolayers and adhesion. Generally, surface science can be divided into surface physics and surface chemistry. Surface physics can be roughly defined as the study of physical changes occurring at interfaces, such as surface diffusion, surface reconstruction, surface phonons and plasmons, epitaxy, surface enhanced Raman scattering, the emission and tunneling of electrons, spintronics and the self-assembly of nanostructures on surfaces and so on. On the other hand, surface chemistry is roughly defined as the study of chemical reactions at interfaces, which is particularly important to the field of heterogenous catalysis. Surface chemistry overlaps with electrochemistry and sometimes with surface physics. When a small molecule hits a solid surface, it may simply either bounce back or be adsorbed. The adsorbed molecules can dissociate into constituent groups or atoms as a result of the strong adsorbate-substrate interaction and can also react directly with surface groups or other previously adsorbed species. Surface chemistry has been brought into the center of chemistry development both because of the intellectual challenge to understand the rich diversity of surface phenomena and because of its importance in chemical and energy conversion technologies.

The study of chemical processes at surfaces and interfaces has a long history. In 1912, P. Sabatier was awarded one half of the Nobel Prize for "his method of hydrogenating organic compounds in the presence of finely disintegrated metals whereby

the progress of organic chemistry has been greatly advanced in recent years". Heterogeneous catalysis was also the central process behind the award of the Nobel Prize to F. Haber "for the synthesis of ammonia from its elements". In 1932, the chemistry prize was awarded to I. Langmuir "for his discoveries and investigations in surface chemistry". C. N. Hinshelwood and N. N. Semenov were given the prize "for their research into the mechanisms of chemical reactions" in 1956. Most recently, in 2007, Gerhard Ertl was awarded the Prize "for this thorough studies of fundamental molecular processes at the gas-solid interface".

The study of surfaces involves both physical and chemical analysis techniques, including X-ray photoelectron spectroscopy (XPS), X-ray absorption spectroscopy (XAS), Auger electron spectroscopy (AES), low-energy electron diffraction (LEED), electron energy loss spectroscopy (EELS), infrared spectroscopy (IR), thermal desorption spectroscopy (TDP), nuclear magnetic resonance (NMR), ion scattering spectroscopy (ISP), just to mention a few.

In 1998, Walter Kohn and John A. Pople shared the Nobel Prize of chemistry "for his development of density-functional theory" and "for his development of computational methods in quantum chemistry". Since last decades, density functional theory (DFT) based first-principles calculation has been widely used to investigate both molecules and condensed matters. The combination of experimental measurements and theoretical calculations has become a powerful tool to reveal the underlying physical and chemical properties of investigated systems. Moreover, it is easier to build ideal models by theoretical calculations than by experiments, therefore, theoretical studies can sometimes provide efficient and meaningful predictions.

In this thesis, I shall concentrate on the explanation of experimental observations by performing DFT calculations. The geometric, electronic and even magnetic properties of adsorbed systems, the reaction mechanisms of simple surface reactions; the structures of core hole electron states are all in the scope of my present work. Surfaces that I have investigated are gold surface, iron oxide ultrathin film, titanium oxide surfaces, and graphene oxide sheets, which are quite important surfaces in present surface chemistry and catalysis. The contents of other parts are arranged as the following:

- briefly introduce the basis idea of DFT in **Chapter 2**.

- present the chemical and electronic properties of adsorbates I am interested in in **Chapter 3**.

- give a outline of the principle of X-ray photoelectron and absorption spectroscopy and the practical technique of theoretical simulation in **Chapter 4**.
- present the results of my works in **Chapter 5**.

In the rest part of this section, I will give some brief introduction about the surfaces investigated in my previous work in **Sec. 1.1** and the spectroscopies used in my work in presented in **Sec. 1.2**.

1.1 Concerned surfaces

1.1.1 Gold Surface

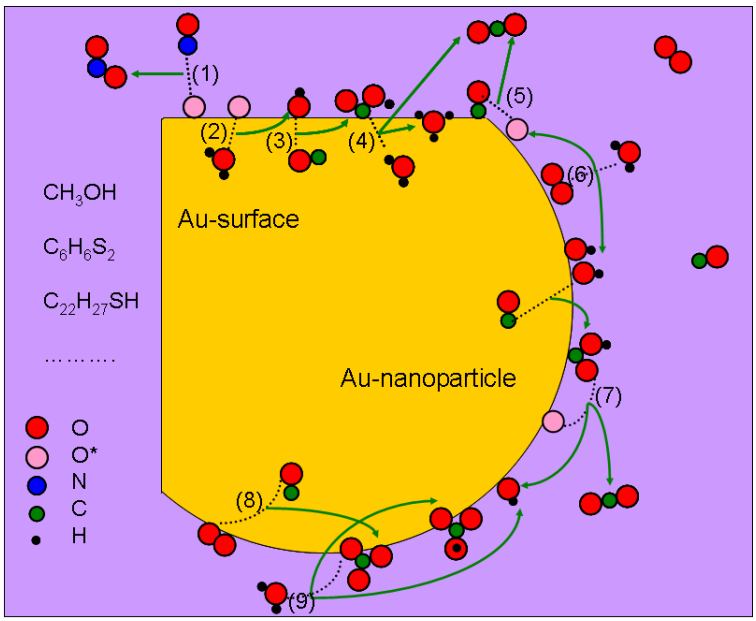

Figure 1.1: *Schematic model for gold related chemistry. The left and top parts represent gold surface and the curve part corresponds to gold nanoparticles. The content of our works are indicated in this figure:* $C_6H_6S_2$, $C_{22}H_{27}SH$ *adsorption on gold surface; NO oxidation on oxygen covered gold surface, CO oxidation on water-oxygen covered gold surface. Also, CO oxidation under the coexistence of moisture on gold nanoparticles shown in other works is also presented in this figure. The numbers represent several possible reaction processes.*

Gold possesses an important position in modern technology. It can be used as electrode of molecular electronics or substrate of self-assemble monolayers etc and

since the work of Haruta and his coworkers [1], the hidden inner beauty of gold as catalyst has been discovered. Nowadays the topic of gold catalysis represents one of the fastest growing field in science. In the past decade, the surprisingly high catalytic activity of Au nanoparticles dispersed on oxide TiO_2[2–4], CeO_2[5, 6], ZrO_2[7, 8], MgO[9, 10], Al_2O_3[11, 12] surfaces has been intensively studied. Au-based catalysts have been widely applied to many important processes such as CO oxidation, partial oxidation of hydrocarbons and selective hydrogenation of unsaturated hydrocarbons, sugar processing and so on.

In the past few years, I have paid special attention to some molecules adsorbed on gold surface such as oxygen, CO, NO, H-saturated carbon clusters (diamondoid), and 1,4-dithiol-benzene. 1,4-dithiol-benzene[13] is a model molecule in molecular device[14–17]. Diamondoid molecules[18–22] are negative electron affinity materials and their self-assemble monolayer on metal surfaces can be used as an electron emission device. CO and NO oxidations are basic examples of catalysis on gold. The oxidation of NO on oxygen covered Au (111) surface and CO oxidation on water-oxygen covered surface are investigated. Moisture plays an important role in CO oxidation process[23]. The presence of water molecules may help the adsorption of oxygen or stabilize the transition state (TS) of elementary steps.

1.1.2 Oxide surfaces

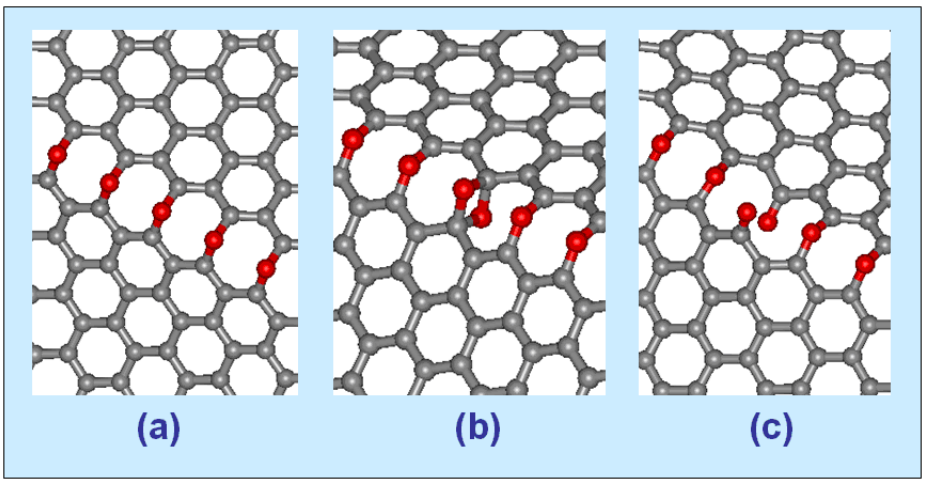

Figure 1.2: *(a) A graphene sheet with an epoxy chain. (b) An epoxy pair or (c) a carbonyl pair is formed in the epoxy chain.*

Another type of surface I interest in is oxide surface, such as, FeO ultrathin film[24–27], rutile TiO_2 (110) surface[28–32], anatase TiO_2 surface[33–38], and graphene oxide[39–47] sheet.

Titanium dioxide (TiO_2) is one of the most investigated metal oxide. It is well known that TiO_2 has a great variety of technological applications in several different areas such as heterogeneous catalysis, photocatalysis, sensoristics, cosmetics, biocompatible coating and so on. In any one of such fields, the understanding of the interaction between TiO_2 surface and different molecules is of primary importance. Among the experimental and theoretical investigations on several species adsorbed on TiO_2, those regarding the interaction between water and the titanium surface have been predominant due to the fundamental role played by water in a large number of chemical and biological processes. Water covered rutile and anatase TiO_2 surfaces are studied by quantum mechanical molecular dynamics (MD) simulation and the different surface species are distinguished by core level shift (CLS) calculations.

Graphene has recently attracted an intense research interest due to its novel physical properties and the great potential in various applications. A big challenge in graphene research is the massive production of high quality samples. Oxidation nowadays becomes an important chemical approach to manipulate graphitic materials. Upon oxidation, graphite readily exfoliates as single sheets in water, forming graphene oxide (GO). Graphene can then be obtained by reducing GO. It is thus important to reveal the structure of GO and its cleavage mechanism.

1.2 X-ray spectroscopies

X-ray photoemission spectroscopy (XPS) is a useful technique to probe both the elemental composition of surfaces and the oxidation state and electronic environment of each component [48–52] by examine the binding energy of core electrons. Quantitative information on elemental composition is obtained from the signal intensities and qualitative information of chemical environment can be derived from the chemical shift of the binding energies of core electrons belonging to a specific element. In general, binding energies increase with the increasing electronegativity of the neighboring atoms. The principles of ultraviolet photoelectron spectroscopy (UPS) are similar to those of XPS, except that ultraviolet radiation (10 to 45 eV) is used instead of soft X-rays (200 to 2000 eV), and what is examined is valence electronic levels [48]. In chapter 4, the principle of X-ray spectroscopies will be introduced.

What I interested in are adsorbates and in my previous works, water covered oxide surfaces, substrate supported gold catalyst, and also the hot graphene oxidehave been investigated. By calculating the ionization potential of atoms in different chemical environments, the peaks in experimental spectra can be assigned and sometimes novel structures have to be proposed to get a better description of experimental data.

X-ray absorption spectroscopy (XAS) is also a useful technique to study the properties of surfaces. The principles of XAS are presented in chapter 4. Nowadays, most of the calculations are performed for isolated molecules, but recently, some groups have extended the simulations by periodic calculations to systems such as liquid water[53–55], diamond bulk, graphite[56], nanotubes[57] and so on. I have performed some tentative work on adsorbates with cluster model or in periodic frame with approximations.

2

Basic method of computational chemistry

2.1 Wavefunction based quantum chemistry

Wave-mechanics, invented by Erwin Schrödinger, is the most popular formulation of quantum mechanics and its essence is the Shrödinger equation. By neglecting some types of interactions and contributions, for example, relativity, the spin-orbital and the spin-spin coupling and so on, the non-relativistic Hamiltonian operator for a many-particle system may be written as a sum of electronic, nuclear and mixed terms as follows:

$$\begin{aligned}\hat{H}_{tot} &= \hat{T}_e + \hat{V}_{ee} + \hat{T}_n + \hat{V}_{NN} + \hat{V}_{Ne} \\ &= -\sum_i \frac{\hbar^2}{2m_e}\nabla^2_{\mathbf{r}_i} + \frac{1}{2}\sum_{i,i'}\frac{e^2}{|\mathbf{r}_i - \mathbf{r}_{i'}|} - \sum_j \frac{\hbar^2}{2M_j}\nabla^2_{\mathbf{R}_j} \\ &\quad + \frac{1}{2}\sum_{j,j'}\frac{Z_j Z_{j'} e^2}{|\mathbf{R}_j - \mathbf{R}_{j'}|} - \sum_{i,j}\frac{Z_j e^2}{|\mathbf{r}_i - \mathbf{R}_j|}\end{aligned} \tag{2.1}$$

In this expression T indicates the kinetic energy, V the potential energy, N and e are the labels for the nuclei and the electrons, respectively. $\mathbf{r}$ and $\mathbf{R}$ are the coordinates of electron and nuclei. The total energy E of the system is derived from the eigenvalue equation:

$$\hat{H}_{tot}\Psi(\mathbf{r},\mathbf{R}) = E\Psi(\mathbf{r},\mathbf{R}) \tag{2.2}$$

All physical quantities of the many-particle system can be obtained from the wave-function $\Psi(\mathbf{r},\mathbf{R})$. Heitler and London's work on hydrogen molecule in 1927 marked the start of quantum chemistry. Theoretically, one can get the solution of any

system, while practically it is a very complex task to accurately resolve the many-particle Shrödinger equation. Several types of approximations are widely adopted for practical application.

It is well known that the nuclei are much heavier than the electrons and therefore the electron movement is much faster than that of nuclei, the nuclear position can thus be assumed as fixed during the electron motion. The separation of the electronic and nuclear motions, is known as the Born-Oppenheimer(BO, adiabatic) approximation. The expression of the electron Hamiltonian can then be simplified as:

$$\hat{H}_e(r,R) = -\sum_i \frac{\hbar^2}{2m_e}\nabla^2_{\mathbf{r}_i} + \frac{1}{2}\sum_{i,i'}\frac{e^2}{|\mathbf{r}_i - \mathbf{r}_{i'}|} - \sum_{i,j}\frac{Z_j e^2}{|\mathbf{r}_i - \mathbf{R}_j|} \tag{2.3}$$

The cases where BO approximation does not work are out of the scope of this thesis.

To solve the Schrödinger equation, it is necessary to work out a convenient representation for the electronic wave function. N-fermions has to obey the Pauli exclusion principle and Fock wrote the wavefunction as a determinant. Considering N individually occupied one-electron states, the wave function Φ is expressed as:

$$\Psi = \frac{1}{\sqrt{N!}}\begin{vmatrix} \phi_1^{\sigma_1}(\mathbf{r}_1) & \phi_2^{\sigma_1}(\mathbf{r}_1) & \cdots & \phi_N^{\sigma_1}(\mathbf{r}_1) \\ \phi_1^{\sigma_2}(\mathbf{r}_2) & \phi_2^{\sigma_2}(\mathbf{r}_2) & \cdots & \phi_N^{\sigma_2}(\mathbf{r}_2) \\ & \vdots & & \\ \phi_1^{\sigma_N}(\mathbf{r}_N) & \phi_2^{\sigma_N}(\mathbf{r}_N) & \cdots & \phi_N^{\sigma_N}(\mathbf{r}_N) \end{vmatrix} \tag{2.4}$$

The elements of the determinant in Eq. 2.4 are spin orbitals, i.e. one electron function obtained as the product of a spatial orbital multiplied by a spin function. By applying the Schrödinger equation Eq. 2.2 to a Slater determinant, and minimizing the spin-orbitals with respect to the energy via a variational method, the total energy of the N-electron system is written as:

$$E = \sum_i^N \epsilon_i - \frac{1}{2}\sum_{ii'}^N (J_{ii'} - K_{ii'}) + V_{nn} \tag{2.5}$$

where ϵ_i are the eigenvalues of one-electron equations, which are also named as Hatree-Fock equations:

$$F_i\phi_i(\mathbf{r}_1) = \epsilon_i\phi_i(\mathbf{r}_1) \tag{2.6}$$

where F_i is the Fock operator, whose form is:

$$F_i = h_i + \sum_{i'}^N (J_{i'} - K_{i'}) \tag{2.7}$$

where h_i is the single electron hamiltonian

$$h_i = -\frac{\hbar^2}{2m_e}\nabla_{r_1}^2 - \sum_j \frac{Z_j e^2}{|\mathbf{r}_1 - \mathbf{R}_j|} \tag{2.8}$$

J and K are electron operators describing the two-electron repulsion and the electron exchange interaction, respectively:

$$J_{i'}|\phi_i(\mathbf{r}_1)\rangle = (\int \phi_{i'}^*(\mathbf{r}_2)\frac{e^2}{r_{12}}\phi_{i'}(\mathbf{r}_2)d\mathbf{r}_2)|\phi_i(\mathbf{r}_1)\rangle \tag{2.9}$$

$$K_{i'}|\phi_i(\mathbf{r}_1)\rangle = (\int \phi_{i'}^*(\mathbf{r}_2)\frac{e^2}{r_{12}}\phi_i(\mathbf{r}_2)d\mathbf{r}_2)|\phi_{i'}(\mathbf{r}_1)\rangle \tag{2.10}$$

In these equations, each electron moves independently with each other in the mean field of other nuclei and electrons. The complex multi-electron problem is simplified as a set of one-electron problems. This is one of the basic approximation of quantum chemistry: one-electron approximation.

The above frame work is named as Hartree-Fock (HF) method, which has been widely applied to not only isolated atom or molecule, but also condensed state as well as to any system of identical particles in a potential. In HF method, the electron correlation is not considered, which will induce an error of 1% for total energy. But this error caused by electron correlation is comparable with electron excitation energy, activation energy and so on, which makes HF not accurate to deal with these problems. To include the electron correlation neglected in HF method, new approaches have been developed, such as Configuration Interaction(CI), multi-configuration self-consistent field (MCSCF). However, these methods are too expensive to apply to large systems.

2.2 Density functional theory

In 1927, H. Thomas and E. Fermi proposed the so-called Thomas-Fermi theory based on the homogeneous electron gas model, in which the electrons do not interact with each other or any external field. They found that the energy of such electronic system is only a functional of the electron density n($\mathbf{r}$). That is how DFT got its name. In 1930, Dirac gave an expression of the energy functional of electrons with exchange interaction in an external field $V_{ext}(r)$:

$$\begin{aligned} E_{TF}[n(\mathbf{r})] &= C_1\int d^3\mathbf{r}n(\mathbf{r})^{5/3} + \int d^3\mathbf{r}V_{ext}(\mathbf{r}) + C_2\int d^3\mathbf{r}n(\mathbf{r})^{4/3} \\ &\quad + \frac{1}{2}\int d^3\mathbf{r}d^3\mathbf{r}'\frac{n(\mathbf{r})n(\mathbf{r}')}{|\mathbf{r}-\mathbf{r}'|} \end{aligned} \tag{2.11}$$

Since Thomas-Fermi-Dirac approach starts from a crude approximation, missing the essential physical details, such as shell structures, it was not widely used.

2.2.1 Hohenberg-Kohn theorem

Modern DFT is based on two theorems of Hohenberg and Kohn [58].

Theorem I: For any system of interacting particles in an external potential $V_{ext}(\mathbf{r})$, the potential $V_{ext}(\mathbf{r})$ is determined uniquely, except for a constant, by the ground state particle density $n_0(\mathbf{r})$.

Corollary I: Since the Hamiltonian is thus fully determined, except for a constant shift of the energy, it follows that the many-body wavefunctions for all state (ground and excited) are determined. Therefore all properties of the system are completely determined given only the ground state density $n_0(\mathbf{r})$.

Theorem II: A universal functional for the energy E[n] in terms of the density n(r) can be defined, valid for any external potential $V_{ext}(\mathbf{r})$. For any particular $V_{ext}(\mathbf{r})$, the exact ground state energy of the system is the global minimum value of this functional, and the density n($\mathbf{r}$) that minimizes the functional is the exact ground state density $n_0(\mathbf{r})$.

Corollary II: The functional E[n] alone is sufficient to determine the exact ground state energy and density. In general, excited states of the electrons must be determined by other means. Nevertheless, the work of Mermin shows that thermal equilibrium properties such as specific heat are determined directly by the free-energy functional of the density.

In Hohenberg-Khon theorem, the Hamitonian of a many-particle system in the external field V_{ext} is:

$$\hat{H} = -\frac{\hbar^2}{2m}\sum_i \nabla_i^2 + \sum_i V_{ext}(\mathbf{r}_i) + \frac{1}{2}\sum_{i\neq j}\frac{e^2}{|\mathbf{r}_i - \mathbf{r}_j|} \tag{2.12}$$

and the corresponding energy functional is written as:

$$E_{HK}[n] = T[n] + E_{int}[n] + \int d^3\mathbf{r} V_{ext}(\mathbf{r})n(\mathbf{r}) \tag{2.13}$$

where T[n] and $E_{int}[n]$ are the kinetic energy and potential energy of interacting system, $V_{ext}(\mathbf{r})$ is the potential of the external field including that due to the nuclei.

2.2.2 Kohn-Sham equation: effective one-electron Approximation

In order to get the specific expressions of the items in Eq. 2.2.1, Kohn and Sham constructed a set of one-electron orbitals (K-S orbitals) by introducing an imaginary non-interaction many-electron system which has the same electron density with the real system[59]. By this assumption, the electron density is defined as:

$$n(\mathbf{r}) = \sum_{\sigma} n(\mathbf{r}, \sigma) = \sum_{\sigma} \sum_{i=1}^{N^{\sigma}} |\phi_i^{\sigma}|^2 \tag{2.14}$$

and the kinetic energy $T = T_s$ (in atomic units) is:

$$T_s = -\frac{1}{2} \sum_{\sigma} \sum_{i=1}^{N^{\sigma}} \langle \phi_i^{\sigma} | \nabla^2 | \phi_i^{\sigma} \rangle = -\frac{1}{2} \sum_{\sigma} \sum_{i=1}^{N^{\sigma}} |\nabla \phi_i^{\sigma}|^2 \tag{2.15}$$

the electrostatic potential is defined as the interaction of the charge density n($\mathbf{r}$)with itself:

$$E_{Hatree}[n] = \frac{1}{2} \int d^3\mathbf{r} d^3\mathbf{r}' \frac{n(\mathbf{r}) n(\mathbf{r}')}{|\mathbf{r} - \mathbf{r}'|}. \tag{2.16}$$

Thus, the total energy functional is expressed as:

$$E_{KS}[n] = T_s[n] + \int d\mathbf{r} V_{ext} n(\mathbf{r}) + E_{Hartree}[n] + E_{xc}[n] \tag{2.17}$$

All the many-body interactions are included in $E_{xc}[n]$. And the expression of $E_{xc}[n]$ is:

$$E_{xc}[n] = \langle \hat{T} \rangle - T_s[n] + \langle \hat{V} \rangle - E_{Hartree}[n] \tag{2.18}$$

where n is a function of spatial position $\mathbf{r}$ and spin σ of electron. From Eq. 2.18, $E_{xc}[n]$ is the energy difference of kinetic energy and internal interaction between real interacting system and imaginary non-interacting system.

Minimization of K-S orbitals with respect to the energy functional via a variational method leads to the famous K-S equation:

$$(-\frac{1}{2}\nabla^2 + V_{ext}(\mathbf{r}) + V_{Hartree}(\mathbf{r}) + V_{xc}(\mathbf{r}))\phi_i = \epsilon_i \phi_i \tag{2.19}$$

where, $V_{ext}(\mathbf{r})$, $V_{Hartree}(\mathbf{r})$ and $V_{xc}(\mathbf{r})$ are external potential, Hartree potential and exchange-correlation potential, respectively. The effective potential V_{eff} defined as

$$V_{eff} = V_{ext} + V_{Hartree} + V_{xc} \tag{2.20}$$

is determined by the electronic density, while the electronic density is defined by the eigenfunction ϕ of Eq. 2.19, so a self-consistent field (SCF) method is used to solve the equation. If the converged electronic density n_0 is obtained, the total energy of the system is expressed as:

$$E_0 = \sum_i^N \epsilon_i - \frac{1}{2}\int d^3\mathbf{r}\int d^3\mathbf{r}'\frac{n_0(\mathbf{r})n_0(\mathbf{r}')}{|\mathbf{r}-\mathbf{r}'|} - \int d^3\mathbf{r}V_{xc}(\mathbf{r})n_0(\mathbf{r}) + E_{xc}[n_0] \quad (2.21)$$

where ϵ_i are the eigenvalues of one-electron KS equations.

KS orbitals are introduced as a mathematical tool to calculate the kinetic energy for a system of N non interacting electrons. In this sense, they do not have a physical significance. While, comparison with experimental data shows that valence K-S orbital energies, very often, well match the measured electronic energy levels. However, the discrepancy increases for core electrons which comes from the more and more important self-interaction of electrons. So self-interaction corrections are needed to get accurate orbital energies[60].

2.2.3 Exchange-correlation functional

LDA and GGA

Mathematically, it would be conceptually possible to reach an exact resolution of the electronic energy functional problem. However, the main difficulty in DFT is that the exact exchange correlation functional is unknown. The development of efficient exchange-correlation functionals is the key for the success of density functional theory. Traditionally, the functionals are separated into an exchange and a correlation part.

The ab initio functionals are built without any parametrization deriving from experimental data. One approach is to develop a functional that only depends on the electron density. This is the case of the exchange functional known as local density approximation(LDA), which treats the density locally as for a homogeneous electron gas. The LDA has evolved into the local spin density approximation (LSDA), where the densities of electrons of different spin are considered independently, which is relevant for open shell systems. The correlation energy functional for a uniform electron gas has been developed by Vosko, Wilk and Nusair (VWN)[61].

The Generalized Gradient Approximation (GGA) goes beyond the LDA approach, by extending the functional dependency to the gradient of the density. Very popular GGA exchange functionals, used in my works, are the Perdew and Wang (PW91)[62], Becke (B88)[63] and PBE[64]. They are built by introducing correc-

tions to the LSDA exchange functionals by adding terms depending on the gradient of the electronic density.

LDA+U

DFT with L(S)DA or GGA approximation has made many successes, while due to insufficient consideration of the on-site Coulomb repulsion, it may fail in describing the electronic structure of strongly correlated materials such as $3d$-transition-metal oxides and rare earth elements and compounds where the electrons tend to be localized and strongly interacting. Various methods have been developed to extend the functional approach to incorporate effects that are expected to be important on physical grounds, for example self-interaction correction (SIC) method and LDA+U approach.

"DFT+U" stands for methods that involve LDA- or GGA-type calculations coupled with an additional orbital-dependent interaction[65, 66]. The additional interaction is usually considered only for highly localized atomic-like orbitals on the same site, i.e. of the same form as the "U" interaction in Hubbard models [67]. The effect of the added term is to shift the localized orbitals relative to the other orbitals, which attempts to correct errors known to be large in the usual LDA or GGA calculations. The approach as formulated by Dudarev[68] is used in our calculation:

$$E_{LSDA+U} = E_{LSDA} + \frac{U-J}{2}\sum_{\sigma}[(\sum_{j}\rho^{\sigma}_{jj}) - (\sum_{j,l}\rho^{\sigma}_{jl}\rho^{\sigma}_{lj})] \tag{2.22}$$

where U and J are the spherically averaged matrix elements of the screened Coulomb electron-electron interaction and ρ^{σ}_{jl} is the density matrix of d electrons. For an individual ion this density matrix is diagonal in the m, m' representation and its eigenvalues equal $n_{m,\sigma}$. DFT+U approach has been successfully applied to NiO [65], CoO[69] and FeO [24]. In my previous work, to investigate the magnetic structure of FeO/Pt(111) ultrathin film, DFT+U is adopted.

2.3 Basis sets

A basis set is a set of functions used to project the molecular orbitals, which are expanded as a linear combination of such functions with the weight or coefficient to be determined. In molecular systems, usually gaussian type atomic orbitals are used. Atomic basis are also used for periodic calculations, which have been implemented in SIESTA and DMol^3. It is efficient to calculate one-dimensional

or 0-dimensional systems. While, local basis sets are not sufficient to calculate diffusive orbitals, for example, in my work of adsorbed diamondoid, DMol^3 gave qualitative incorrect results.

While for periodic boundary conditions, such as bulk material or surfaces, plane wave basis sets with a kinetic energy smaller than E_{cut} are always adopted:

$$|\mathbf{G}+\mathbf{k}| < G_{\text{cut}} \qquad \text{with} \qquad E_{\text{cut}} = \frac{\hbar^2}{2m} G_{\text{cut}}^2$$

where $\mathbf{G}$ is the wave vector of plane wave and $\mathbf{k}$ is the vector in reciprocal space.

This technique has been implemented in some codes such as VASP[70–73], PWSCF, CPMD and so on. VASP is widely used in my works.

2.4 Pseudopotential

Usually, it needs quite a large number of basis functions to describe core electron wave function for its strong oscillator, especially with plane wave basis sets. Thus, the computational effort will increase a lot. To reduce computational effort, substitutional methods, such as "pseudopotential", are implemented. The fundamental idea of a "pseudopotential" is to replace the strong Coulomb potential of the nucleus and the effects of the tightly bound core electrons by an effective ionic potential acting on the valence electrons. A pseudopotential can be generated in an atomic calculation and then used to compute properties of valence electrons in molecules or solids, since the core states remain almost unchanged. Furthermore, the fact that pseudopotentials are not unique allows the freedom to choose forms that simplify the calculations and the interpretation of the resulting electronic structures.

Popularly used "pseudopotentials" includes "ab inito norm-conserving" (NCPP), "ultrasoft" pseudopotentials (USPP) and also projected augmented wave (PAW) method. They have led to accurate calculations that are the basis for much of the current research and development of new methods in electronic structure.

It is also possible to get all-electron orbitals from "pseudopotential", which is useful to deal with core orbital related projects. Recently, R. Car *et al.* reconstructed the frozen-core all-electron orbitals from pseudo-orbitals [74], such as USPP and PAW.

In my works, USPP[75] or PAW[76] methods implemented within plane wave basis are adopted to investigate the properties of concerned systems.

3

Simulation of various properties

3.1 Molecular dynamics

Molecular dynamics (MD) is a specialized discipline of molecular modeling and computer simulation based on statistical mechanics; the main justification of the MD method is that statistical ensemble averages are equal to time averages of the system, known as the ergodic hypothesis. According to the approach to get the total energy, molecular dynamics can be divided into classical molecular mechanic molecular dynamics (MM MD), quantum mechanic molecular dynamics (QM MD) and the combined QM/MM. QM/MM is totally out of the scope of my works.

In classical molecular dynamics simulations, the potential parameters are obtained from experiments or by fitting the bond energies or bond angles got from first principles calculations. The analytic form of potentials are efficient and cheap, which make it possible to apply classical MD to large systems, such as protein folding, interaction of biomolecules and surfaces (In **Paper VII**) and so on. However, for the absence of electronic information, the potentials are not exact and empirical potential can only be used to given atomic or molecular systems and also it is hard to describe bond forming and breaking. If more accurate descriptions are needed, we should turn to quantum molecular dynamics simulations.

According to Born-Oppenheimer approximation, the forces acting on nucleus are given by Hellmann-Feynman theorem:

$$\mathbf{F}_I(t) = M_I \ddot{R}_I(t) = \nabla_I \min_{\Psi_0} \{\langle \Psi_0 | H_e | \Psi_0 \rangle\} \tag{3.1}$$

$$E_0 \Psi_0 = H_e \Psi_0. \tag{3.2}$$

where, $\mathbf{F}_I$, M_I and R_I are the force on nucleus I, the mass and the position of nucleus I, respectively. H_e and Ψ_0 are the Hamitonian and the ground state wave-

function of the electronic system. Energy is a function of both electronic wavefunctions and nuclei coordinates. Once the energy functional reaches the minimum depending on the electronic wavefunction, the system reaches the Born-Oppenheimer potential surface and the molecular dynamics starts. The conventional numerical algorithm is Verlet algorithm:

$$\mathbf{R}_i(t+\Delta t) = \mathbf{R}_i(t) + \mathbf{v}_i(t)\cdot\Delta t + \frac{\mathbf{F}_i}{2M_i}\cdot(\Delta t)^2 \tag{3.3}$$

$$\mathbf{v}_i(t+\Delta t) = \mathbf{v}_i(t) + \frac{\mathbf{F}_i(t+\Delta t)+\mathbf{F}_i(t)}{2}\cdot\frac{\Delta t}{M_i} \tag{3.4}$$

Based on the positions and forces at time t, the equations of motion are numerically solved and we can get the position and momentum at time $t+\Delta t$. Then the trajectories in phase space are obtained.

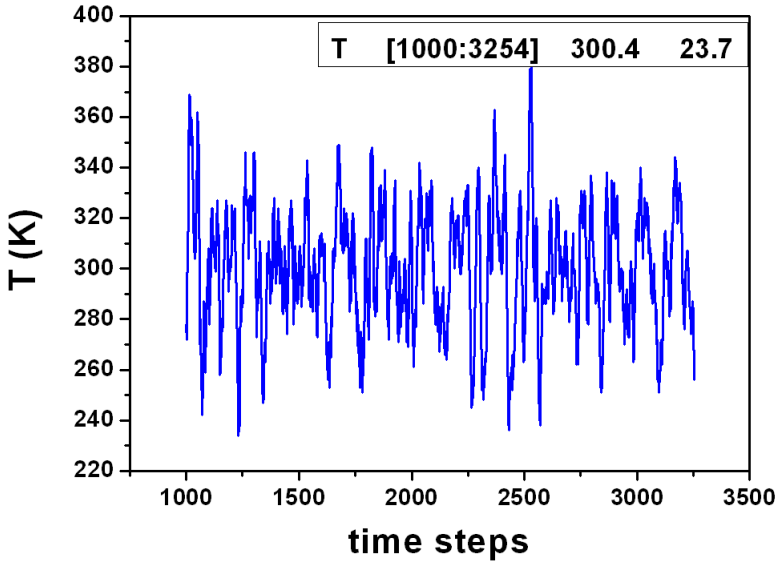

Figure 3.1: *Temperature vs time during the MD simulation at equilibrium state.*

According to different practical conditions under which experiments being performed, various type of simulations can be adopted, such as, constant temperature, constant pressure or constant energy. Till now, quantum molecular dynamics can manage about hundreds of atoms with several picosecond (ps) time scale. Regarding constant temperature simulation, when the system reaches equilibrium, the standard deviation (Δ) of temperature should be less than $T_{target}/\sqrt{n_{free}}$. In previous work, I have performed constant temperature quantum molecular dynamics simulations for oxide adsorbed systems in **Paper VI**, **Paper VII** and **Paper VIII**. In Figure 3.1, the temperature at different time t at equilibrium state is presented.

3.2 Vibrational surface spectroscopy

Vibrational spectroscopy provides the most definitive means of identifying the surface species generated upon molecular adsorption or the species generated during surface reactions. In principle, any technique that can be used to obtain vibrational data from solid state or gas phase samples can be applied to the study of surfaces; in addition there are a number of techniques which have been specially developed to study the vibrations of molecules at interfaces. There are, however, only two techniques that are routinely used for vibrational studies of molecules on surfaces, these are:
1. Infrared Spectroscopy (of various forms, e.g. Reflection-Absorption Infrared Spectroscopy (RAIRS))
2. Electron Energy Loss Spectroscopy (EELS or high resolution electron energy loss spectroscopy (HREELS)).
RAIRS has excellent energy resolution ($< 2\ cm^{-1}$), which is useful for separating multiple peaks, phase transition, lateral interactions, dynamics of coupling. But it cannot observe modes less than 800 cm^{-1} and only dipole active modes (component perpendicular to surface) can be detected. It is less sensitive than HREELS, which is more capable of working on very highly-absorbing adsorbates such as CO or NO. HREELS is based on multiple scattering mechanism which allow observation of modes parallel and perpendicular to surface. It can observe modes in a wide range $0 \rightarrow 4000\ cm^{-1}$ and perform vibrational and electronic loss spectroscopy. But the resolution of HREELS is $6 - 8\ cm^{-1}$, which is lower than that of RAIRS.

Usually, finite differences method is used to calculate the vibrational frequencies of adsorbates. Each atom is displaced along the +/- direction of Cartesian axis and the frequency spectum and corresponding normal modes can be obtained by diagonalizing the dynamical matrix. The vibrational frequencies of different surface species such as NO, CO , HOCO and so on. are calculated in **Paper I** and **Paper II**.

3.3 Scanning tunneling microscopy

Scanning tunneling microscopy (STM) is a powerful technique for observing surfaces at atomic level, which can be used not only in ultrahigh vacuum but also in air and in various other liquid or gas ambient and at temperature range from near zero to several hundreds Kelvin. STM probes the density of states of a system using tunneling current. The resolution of STM can be achieved 0.1 nm lateral and 0.01 nm depth [77]. During measurement, a tip is brought into close proximity

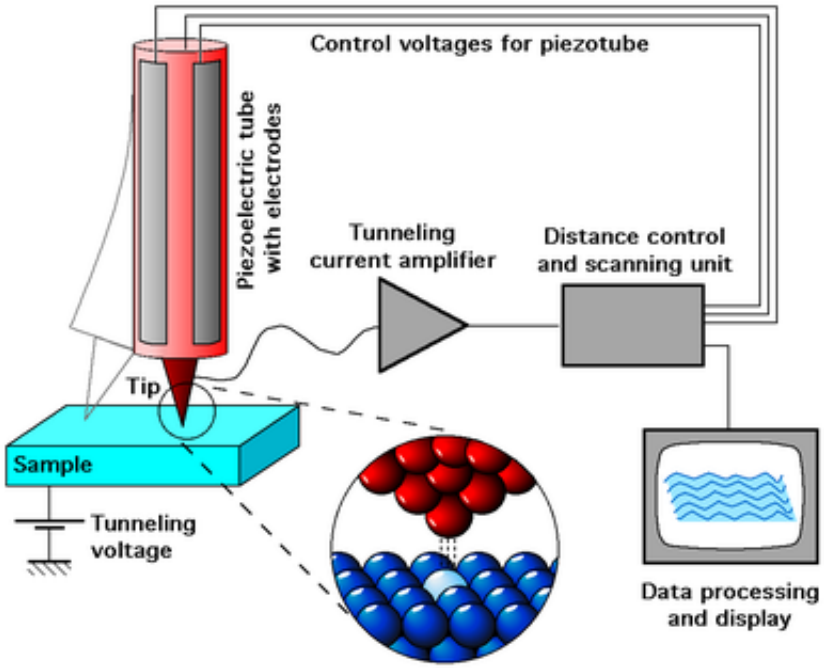

Figure 3.2: *Scheme view of STM. Taken from internet.*

of the sample by some coarse sample-to-tip control. The common sample-to-tip distance (W) is maintained as 4-7 Å, which is the equilibrium position between attractive ($3 < W < 10$ Å) and repulsive ($W < 3$ Å) interactions. Once tunneling is established, piezoelectric transducers are implemented to move the tip in three directions. Generally, there are two modes in STM measurements: constant height mode and constant current mode. The former mode means during measurement, the tip is scanning across the sample in the x-y plane with certain height and the change in current with respect to position can be recorded. While, the latter one represent the measurement is performed with a constant current by varying the tip height. In addition to scanning across the sample, information on the electronic structure of the sample can be obtained by sweeping voltage and measuring current at a specific location. This type of measurement is called scanning tunneling spectroscopy (STS).

In theoretical simulation, time-dependent perturbation theory developed by Bardeen successfully describe the tunneling process of STM. Within the Bardeen approach, the wavefunction of the single electron state of the surface (ψ_s) and tip(χ_t) are resolved from Schrödinger equations of separated sample and tip. The tunneling

matrix element M_{st} is written as:

$$M_{st} = \frac{\hbar^2}{2m} \int_{\sum} [\chi_t^*(\vec{r}) \nabla \psi_s(\vec{r}) - \psi_s^*(\vec{r}) \nabla \chi_t(\vec{r})] d\vec{S} \tag{3.5}$$

where $\sum$ is a interface between surface and tip. Then the tunneling probability from ψ_s to χ_t can be given by Fermi golden rule:

$$W_{st} = \frac{2\pi}{\hbar} |M_{st}|^2 \delta(E_s - E_t) \tag{3.6}$$

The total tunneling current between a surface and a tip is described by the sum over surface and tip state as follows:

$$I = \frac{2\pi}{\hbar} \int_{-\infty}^{+\infty} [f(E_F - eV + \epsilon) - f(E_F + \epsilon)] \times \rho_s(E_F - eV + \epsilon) \rho_t(E_F + \epsilon) |M|^2 d\epsilon \tag{3.7}$$

where $f(E) = \{1 + \exp[(E - E_F)/k_B T]\}^{-1}$ is the Fermi distribution function, and ρ_s, ρ_t is the density of states of sample and tip. The bias voltage between surface and tip equals V, and the integration surface is assumed to be in the vacuum region. If $K_B T$ is smaller than the energy resolution in STM measurement, the tunneling current can be simplified as:

$$I = \frac{2\pi}{\hbar} \int_{0}^{eV} [\rho_s(E_F - eV + \epsilon) \rho_t(E_F + \epsilon)] |M|^2 d\epsilon \tag{3.8}$$

And if we suppose that the tunneling matrix elements keep almost constant in the region we are interested at, Eq. 3.8 can be further simplified as:

$$I \propto \int_{0}^{eV} [\rho_s(E_F - eV + \epsilon) \rho_t(E_F + \epsilon)] d\epsilon \tag{3.9}$$

Based on Bardeen approach, Tersoff and Hamann find a way to explain STM images by tunneling current calculation. They got:

$$I = 0.1 R^2 V \exp^{2\kappa R} \rho(\mathbf{r}_0, E_F) \tag{3.10}$$

the units for distance and energy are a.u and eV. In which, $\kappa = \sqrt{2m\Phi}/\hbar$, Φ and ρ are work function and local density states of sample. Eq. 3.10 suggests that what we get from constant current mode is the contour of local density of sample. Tersoff-Hamann approximation is a special case for Bardeen approach, which has been successfully applied to interpret STM images. For the cases where Tersoff-Hamann approximation[78] does not work, we have to return to Bardeen approach.

Based on Tersoff-Hamann approximation, the STM images under different bias of FeO/Pt(111) ultrathin film are well reproduced in **Paper V**.

Scanning tunneling spectroscopy (STS) is adopted to study local electronic structures of surfaces. From Eq. 3.9, it can be derived:

$$\frac{dI}{dV} \propto \rho_s(E_F - eV + \epsilon)\rho_t(E_F + \epsilon) \tag{3.11}$$

3.4 Surface reaction

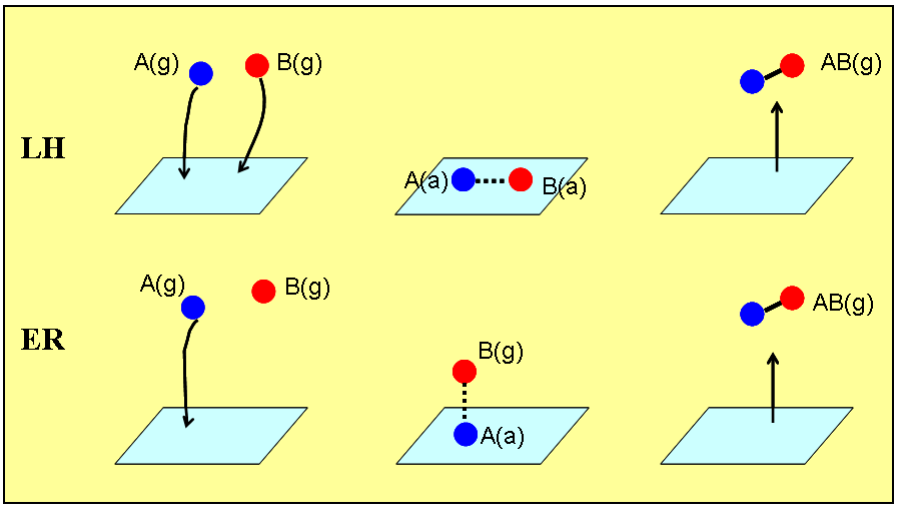

Figure 3.3: *Schematic representation of surface reaction mechanisms: Langmuir-Hinshelwood, where both molecules are adsorbed on the surface and then they undergo a chemical reaction, and Eley-Rideal, where only one molecule is adsorbed on the surface and the other one reacts directly with it, without adsorbing.*

Heterogeneous catalysis is the term used to refer to catalytically activated chemical reaction, where the catalyst is in a different phase with respect to reactants. Overall heterogeneous catalytic reaction is composed of several elementary steps, which are the adsorption of reactants on the surface, diffusion on the surface, reaction steps involving bond breaking and bond making, so as to form product molecules, and final desorption of products.

Two kinds of mechanism through which surface reactions can proceed are schematically represented in Figure. 3.3: the Langmuir-Hinshelwood (LH) and the Eley-Rideal (ER) mechanism. In the former case, both molecules are adsorbed on the surface and then they react to form products. A typical example of chemical reaction which proceeds through a LH mechanism is the carbon monoxide oxidation

to form carbon dioxide on platinum catalysts. In the ER mode, only one molecule is adsorbed on the surface and the other one reacts directly with it, without adsorbing. The reaction of NO with pre-adsorbed oxygen on Au catalyst to form NO_2 gas is an example of reaction proceeding through an ER mechanism. In substrate involved surface reaction, another mechanism named as Mars-van Krevelen mechanism can also be proceeded [79].

The most important thing in studying surface reaction is to find the transition state (TS), which plays a decisive role in the understanding and design of chemical reactions, of each elementary step. Despite their fundamental significance, transition state structures are very challenging to locate accurately and conventional algorithms are typically computationally demanding and are not universally applicable. Over the last several years a number of methods have been proposed to locate transition state structures.

3.4.1 Constraint minimization method: drag method

The simplest and perhaps the most intuitive method may be *drag method*[80]. One degree of freedom is chosen as the drag coordinate, which is held fixed while all the other degrees of freedom are relaxed. The drag coordinate is increased by successive small steps and the system is dragged from reactants to products. The maximum energy during all the step points is taken to be the saddle point energy. A good reaction coordinate chosen to be the drag coordinate could be the distance between two atoms, or the angle formed by three atoms and so on. If it is not easy to find such an intuitive choice, the drag coordinate can be simply chosen as the straight line interpolation between the initial and the final states, which is a less biased way and in principle all coordinates of the system contribute to the drag coordinate.

But that both the intuitive reaction coordinate and the unbiased straight line interpolation can be turned out to be bad reaction coordinates[81, 82]. These choices can well represent the difference between reactants and products, which is not enough to be a reaction coordinate. A good reaction coordinate should give the direction of the unstable normal mode at the saddle point and then the minimization of all the other degrees can bring the system to the saddle point. This method is used to estimate the reaction energy of NO oxidation in **Paper I**

3.4.2 Linear and quadratic synchronous transit method

Linear Synchronous Transit (LST) [83] is another commonly used method to find the transition state by interpolating geometrically between a reactant and a product to generate a reaction pathway. In the original LST method[83], a set of structures connecting reactant and product are obtained by linearly interpolating the distances between pairs of atoms in the reactant and product according to:

$$r_{ab}^{i}(f) = (1-f)r_{ab}^{R} + fr_{ab}^{P} \tag{3.12}$$

where r_{ab}^{R} and r_{ab}^{P} are the inter-nuclear distances between the pair of atoms a and b in the reactant and the product, respectively and where f is an interpolation parameter which varies between 0 and 1.

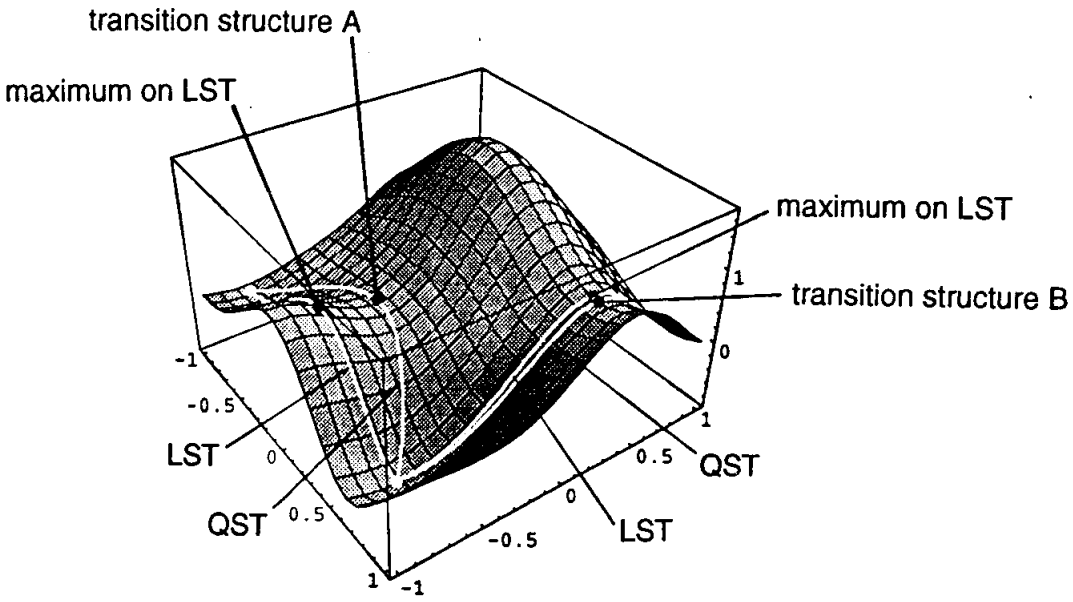

Figure 3.4: *Scheme of the difference of LST and QST. Taken from internet, if anyone knows the reference please let me know.*

For the number of distinct inter-nuclear separation in a molecule with N atoms, N(N-1)/2, is usually greater than the degrees of freedom 3 N, Eq. 3.12 over specifies the geometry. Halgren and Lipscomb define a function S:

$$S(f) = \frac{1}{2}\sum_{a\neq b}\frac{[r_{ab} - r_{ab}^{i}(f)]^2}{[r_{ab}^{i}(f)]^4} + 10^{-6}\sum_{a}[x_a - x_a^{i}(f)]^2 \tag{3.13}$$

where x_a^i is the interpolated Cartesian position of an atom and x_a is the actual coordinate. S is always greater or equal to zero and the reactant and product

geometries will minimize S when f is 0 and 1, respectively. The LST pathway is generated by computing the geometries for several values of f. Such an interpolation is purely geometrical without energy information. When DMol^3 is used to perform an LST search along a given pathway, the maximum total energy as a function of f is located. This is the LST approximation to the transition state. In periodic systems idealized LST paths are defined by a straightforward generalization of Eq. 3.12. However, a modified functional form for S is used,

$$S(f) = \frac{1}{2}\sum_{a,b,R}(r_{ab+R} - r^i_{ab+R})^2\omega(r^i_{ab+R}(f)) + 10^{-6}\sum_a[x_a - x^i_a(f)]^2 \qquad (3.14)$$

where

$$\omega(r^i_{ab}) = 0 \qquad : a = b. \qquad (3.15)$$

$$\omega(r^i_{ab+R}(f)) = \frac{1}{(r^i_{ab+R}(f))^4} \qquad : a \neq b, R = 0. \qquad (3.16)$$

$$\omega(r^i_{ab+R}(f)) = \frac{1}{(r^i_{ab+R}(f))^4} - \frac{1}{r^4_{cut}} \qquad : r_{ab+R}(f) < r_{cut}, a \neq b, R \neq 0. \qquad (3.17)$$

$$\omega(r^i_{ab+R}(f)) = 0 \qquad : r_{ab+R}(f) > r_{cut}. \qquad (3.18)$$

in which a cutoff radius r_{cut} is introduced. The cutoff radius causes the contributions to S to reduce gradually to zero. Summations over only a few (3-4) unit cells are required to converge S to its asymptotic value.

Quadratic Synchronous Transit (QST) method alternates searches for an energy maximum with constrained minimization in order to refine the transition state to a high degree in which minima perpendicular to the LST are connected as shown in Figure 3.4.

The method used in this thesis (in **Paper II** and **Paper X**) is the complete LST/QST method. First, the energies of the reactant and product structures are computed. Using these two energy points, the maximum along the LST path is searched. Once this maximum is found, a conjugate gradient (CG) optimization of this structure is performed. If the residual forces fall below a specified tolerance, the calculation is considered converged and should be further analyzed. If not, a new maximum is searched along the QST path connecting reactant, product and current best transition state structure. A new CG optimization cycle is then initiated until convergence is achieved.

Once convergence has been achieved, the vibrational spectrum of the predicted transition state structure should have exactly one mode with negative vibrational frequency ν_{TS}. Since the transition state is characterized by a saddle point on the energy hypersurface, the eigenmode corresponding to ν_{TS} illustrates the directions in which the system would evolve away from this saddle point, following the minimum energy reaction pathway.

3.4.3 Nudged elastic bands method

Another widely used method is "NEB"(and developed "CI-NEB"). It is not connected to the works presented in the publication list, but it will be adopted in our ongoing works. In this method, N images are inserted between reactants and products and the Minimum Energy Path (MEP) between initial and final states is characterized by having vanishing forces in the direction perpendicular to the path at each point:

$$\mathbf{F}_{i,\perp} = \mathbf{F}_i - \hat{\tau}_i[\hat{\tau}_i \cdot \mathbf{F}_i] = -\nabla V(\mathbf{x}_i) + \hat{\tau}_i[\hat{\tau}_i \cdot \nabla V(\mathbf{x}_i)] = 0 \quad (3.19)$$

$$\hat{\tau}_i = \frac{\mathbf{x}_{i+1} - \mathbf{x}_i}{|\mathbf{x}_{i+1} - \mathbf{x}_i|} \quad (3.20)$$

where V is the potential energy surface and $(\mathbf{x}_i)$ are the coordinates of image i, with i=1,....,N, and a possible approximation of the tangent $\hat{\tau}_i$ is given. This set of coupled equations can be solved in an iterative way. Total energy and force orthogonal to the path are calculated for each image. The position of corresponding image changes until the $F_{i,\perp}$ on it vanishes and the minimum perpendicular to the path is found. Schematic representation of the methods used to identify MEP and TS on a one-dimensional PES is indicated in Figure 3.5. In order to avoid the collapse to closest local minimum of each image, an elastic interaction[85] between nearest neighbor images is introduced, which keeps the images approximately equal spaced along the path. Only the component of the elastic force parallel to the path, $F_{\parallel}^{el}$, is allowed to act on the images, whose dynamics is now determined by a total force **F**:

$$\mathbf{F}(\mathbf{x}_i) = \{-\nabla V(\mathbf{x}_i) + \hat{\tau}_i[\hat{\tau}_i \cdot \nabla V(\mathbf{x}_i)]\} + \{-k[(2\mathbf{x}_i - \mathbf{x}_{i+1} - \mathbf{x}_{i-1}) \cdot \hat{\tau}_i]\hat{\tau}_i\} \quad (3.21)$$

where k is the elastic force constant. In Eq. 3.4.3, the first contribution is the force perpendicular to the path due to the potential energy surface and the second contribution is the elastic force parallel to the path. In order to have a higher density of images and a better description of the path around the TS, k for images closer to the TS is defined to be stronger than other images. This method is named as nudged elastic bands (NEB).

Among all the images only one will be exactly at TS, which corresponds to the saddle point along the MEP, thus *Climbing Image* (CI) NEB [86] has been developed. Within the CI-NEB, the image closest to the TS is chosen to climb the hill and to approach the TS. The image does not feel the elastic force and its dynamics is determined by a force F:

$$\mathbf{F}(\mathbf{x}_{C-I}) = -\nabla V(\mathbf{x}_i) + 2\hat{\tau}_i[\hat{\tau}_i \cdot \nabla V(\mathbf{x}_i)] \quad (3.22)$$

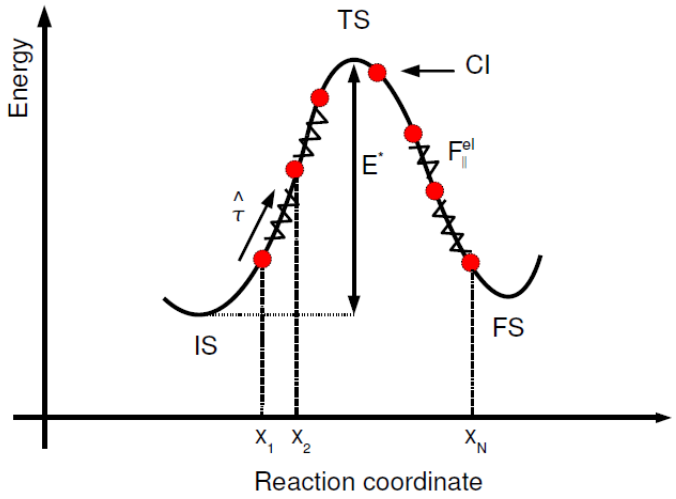

Figure 3.5: *Schematic representation of the methods used to identify MEP and TS on a one-dimensional PES. Red points correspond to N images between IS and FS, connected by springs. CI: climbing image; $\hat{\tau}$: versor tangent to the path; $F_{\parallel}^{el}$:elastic force parallel to the path. Taken from Ref. [84]*

.

where the component parallel to the path is now reversed. The climbing image therefore moves toward a minimum in the direction perpendicular to the path, and toward a maximum along the path, which corresponds to move exactly toward a saddle point.

4

Soft X-ray spectroscopy

The electrons of an atom are divided into valence electrons and core electrons. Core electrons localize around the atomic center and are almost inert in chemical reactions, which provides a method to locally study the electronic properties centered on an atomic site. X-rays, for the high energy, provide an optimal mean to explore atomic and molecular inner shell (core) processes. Regarding different core hole processes, X-ray spectroscopies can be divided into two classes: core-hole creation (X-ray photoemission spectroscopy(XPS), X-ray absorption spectroscopy (XAS or NEXAFS)) and core-hole decay (X-ray emission spectroscopy (XES), Auger emission spectroscopy (AES)). Schematic diagrams of processes involved in X-ray spectroscopies are shown in Figure 4.1.

In this thesis, only theoretical XAS and XPS simulations are applied to investigate isolated molecules or adsorbates (in **Paper VI, VIII**). In the X-ray absorption process the incoming X-ray photon is absorbed and an electron from an inner shell is transferred into an unoccupied state in the valence band. The energy distribution of the excitation probability into unoccupied orbitals forms the XAS spectrum. If the energy of the photon $\hbar\omega$ is larger than the core electron ionization potential (IP), the electron is removed completely from the molecule (transferred to a continuum state given asymptotically by a Coulomb wave in the presence of a core-hole potential). Here, the kinetic energy distribution of ionized core electrons forms the photoelectron spectrum.

In general, the probability per unit time of a transition between an initial state Φ_i and a final state Φ_f is given by the Fermi Golden Rule:

$$P_{i\to f} = \frac{2\pi}{\hbar}|\langle\Phi_f|\bar{V}|\Phi_i\rangle|^2\delta(E_i - E_f + \hbar\omega) \tag{4.1}$$

where $\bar{V}$ is the operator describing the interaction between radiation and matter[87] and E_i and E_f are the electron energies of the initial and final states. The argument

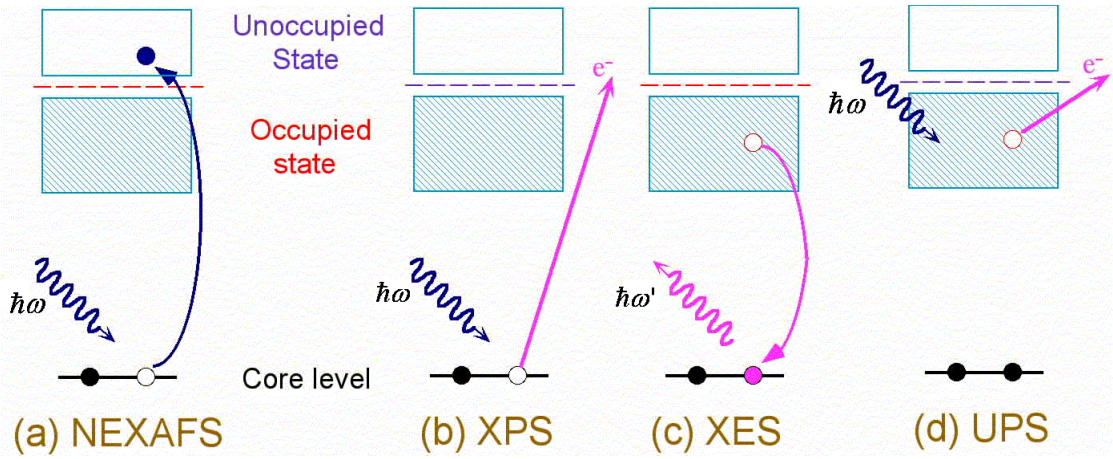

Figure 4.1: *Schematic representation of X-rays processes in an atom or in a molecule. The processes illustrated here are simple one-electron pictures. Taken from the homepage of our department.*

of the δ function derives from the conservation of energy, and tells that this is an absorption process, such that the excitation energy $\hbar\omega$ equals the difference: $E_f - E_i$. It is interesting to observe that the minus sign in front of the photon energy $\hbar\omega$ in the above expression, would have indicated an emission process, in which an electron decays into a level with higher binding energy. In the case of the photoelectric effect, the final state corresponds to an out-coming free electron, and the argument of the δ function turns into:

$$\delta(E_i - E_f + \hbar\omega) = \delta(\hbar\omega - E_B - \frac{p_e^2}{2m_e}) \tag{4.2}$$

where m_e is the electron mass, p_e the electron momentum, and E_B is the binding energy of the electron.

The dominant perturbative describing the interaction of spinless particles of charge -e and mass m_e with an electromagnetic filed is given by

$$V(t) = \frac{e}{mc}\mathbf{A}\cdot\mathbf{p} \tag{4.3}$$

where $\mathbf{p} = \sum \mathbf{p}_i$ is the sum of the linear momentum operators of the electrons and $\mathbf{A}$ is the vector potential[88]. The vector potential of a monochromatic plane wave has the form:

$$\mathbf{A}(r,t) = \mathbf{e}A_0\cos(\mathbf{k}\cdot\mathbf{r} - \omega t) = \mathbf{e}\frac{A_0}{2}(e^{i(\mathbf{k}\cdot\mathbf{r}-\omega t)} + e^{-i(\mathbf{k}\cdot\mathbf{r}+\omega t)}) \tag{4.4}$$

where $\mathbf{e}$ is the polarization unit vector of the photon electric field. From this expression, and by applying the time dependent perturbation theory, one can obtain

a formulation for the potential $\bar{V}$ that represents the transition operator for the absorption (or emission) of a single photon. Its expression is:

$$\bar{V} = e^{i\mathbf{k}\cdot\mathbf{r}}\mathbf{e}\cdot\mathbf{p} \tag{4.5}$$

Since in an atomic transition the wavelength of the radiation is larger than the atomic dimensions, the exponential term can be approximated by a series expansion that can be truncated at the first term by considering dipole approximation[89]:

$$e^{i\mathbf{kr}} = \sum_{n=0}^{\infty} \frac{i^n}{n!}(\mathbf{k}\cdot\mathbf{r})^n \approx 1 \tag{4.6}$$

The inclusion in this expression of higher order terms, corresponds to considering multipole transitions. The dipole approximation leads to a simplified formula for the operator $\bar{V}$, and the transition matrix (d_{fi}) becomes

$$d_{fi} = \langle\Phi_f|\mathbf{e}\cdot\mathbf{p}|\Phi_i\rangle \tag{4.7}$$

in the momentum operator representation and by use of operator equivalents for the total linear momentum operator

$$\mathbf{p} = m\mathbf{v} = -i\hbar\nabla = \frac{im(E_f - E_i)}{\hbar}\mathbf{r} \tag{4.8}$$

and $E_f - E_i = \hbar\omega$, we can get the transition matrix in position operator representation,

$$d_{fi} = im\omega\langle\Phi_f|\mathbf{e}\cdot\mathbf{r}|\Phi_i\rangle \tag{4.9}$$

The resulting expression for the transition probability is:

$$P_{i\to f} = \frac{2\pi}{\hbar}\frac{A_0^2}{4}\frac{e^2\omega^2}{c^2}|\langle\Phi_f|\mathbf{r}|\Phi_i\rangle|^2\delta(E_i - E_f + \hbar\omega) \tag{4.10}$$

where the transition operator (or dipole operator) is simplified as $\mathbf{r}$, which is accepted in a large number of cases as a good operative approximation for the description of one-electron transitions in the spectroscopies. There are many situations, however, when a description beyond the dipole approximation is desired.

An important quantity related to photo-absorption is the cross section (σ), that is a measure of the number of electrons excited or ionized per unit time, divided by the number of impinging per unit area and per unit time. Within the dipole approximation, the absorption cross section takes the form:

$$\sigma = \frac{4\pi^2\hbar^2}{m^2}\frac{e^2}{\hbar c}\frac{1}{\hbar\omega}|\langle\Phi_f|\mathbf{e}\cdot\mathbf{p}|\Phi_i\rangle|^2\delta(E_i - E_f + \hbar\omega) \tag{4.11}$$

The δ function, in general, has a peak when the photon energy $\hbar\omega$ coincides with an electron transition energy. The intensity of the resonances in NEXAFS is expressed by the oscillator strength f, which is the energy integral of the photoabsorption cross section:

$$f = \frac{2}{m\hbar\omega}|\langle f|\mathbf{e}\cdot\mathbf{p}|i\rangle|^2 \tag{4.12}$$

or in the position operator representation:

$$f = \frac{2m\omega}{\hbar}|\langle|\mathbf{e}\cdot\mathbf{r}|i\rangle|^2 \tag{4.13}$$

The discrete and continuum oscillator strengths satisfy Thomas-Reiche-Kuhn sum rule. It states that for a given electron in an atom or molecule the sum of the oscillator strengths of all transitions to all other states, discrete and continuous, occupied and unoccupied, is unity. It then follows that the total oscillator strength for the electronic excitation of an atom or molecule is equal to the number of electrons N in the atom or molecule, i.e.,

$$\sum_n f_n + \int_{IP}^{\infty} \frac{df(E)}{dE} dE = N \tag{4.14}$$

4.1 X-ray photoelectron spectra

If the energy $h\omega$ photon interacting with an atom or a molecule is higher than the ionization potential (IP) of the electron, the latter gets excited into the continuum, i.e. ionized: this is the photoelectric effect. In this thesis, both isolated molecules and adsorbed systems are investigated.

A reformulation of the energy conservation law leads to

$$E_k - \Phi = \hbar\omega - (E_f^{N-1} - E_i^N) = \hbar\omega - E_b \tag{4.15}$$

where E_b is the (exact) definition of the binding energy for the (N-1) electron final state (E_f^{N-1} - E_i^N). The work function Φ is used for metal systems where the binding energy is measured relative to the Fermi level, while, for gas-phase the binding energy is related to the vacuum level, thus $\Phi = 0$. The dipole transition element in the BO and sudden approximation is given as a product of a one electron dipole moment and two overlap integrals

$$\langle f|r|i\rangle \propto \langle\Phi_f^{N-1}|\Phi_i^{N-1}\rangle\langle\phi_c|r|\phi_e(E_k)\rangle\langle\Phi_f(R)|\Phi_i(R)\rangle \tag{4.16}$$

where Φ_f^{N-1} represents the electron configuration of the (N-1) electron system in the presence of the core-hole, Φ_i^{N-1} for the (N-1) electron system in the frozen ground state configuration, ϕ_c the core-electron orbital and $\phi_e(E_k)$ the continuum electron wave function. The last term is the Franck-Condon overlap. The distribution of the core-excited electrons is proportional to the square of this total transition element subject to the energy conservation law. The lifetime of the core-hole can lead to a Lorentzian broadening according to the Heisenberg uncertainty principle. Apart from the chemical sensitivity deriving from the ionization of core electrons, XPS has an important property, namely the surface sensitivity. Electrons that travel through a solid are subject to inelastic scattering events (i.e. low energy excitations). The information depth is given by the universal curve for the electron mean free path, which is $\sim$ 10 Å for 50 eV electrons and increases slowly to about 20 Å for 500 eV electrons.

In this thesis, we focus on applying XPS theoretical calculations to determine surface species and also distinguish chemical environment for element, for example, carbon, oxygen and nitrogen. We prefer to determine the binding energy as core level shift (CLS) according to an energy reference system.

4.1.1 Theoretical method

Initial state approximation

Koopmans' theory provides the simplest way to describe XPS in the independent particle approximation: the final orbital is considered as unaffected by the core-hole. The core level shift is defined as:

$$E_{CLS}^{IS} = -\epsilon_k + \epsilon_k^{ref} \tag{4.17}$$

For atoms or molecules, ϵ is the orbital energy obtained from Hartree-Fock calculations, while for solid ϵ is calculated with respect to Fermi-level. In this picture, all final state effects are neglected and relaxation is important for core hole ionization. Within DFT frame, the eigenvalues of the Kohn-Sham orbitals strictly speaking do not have any physical meaning. Recently, Carravetta et. al. proposed a simple self-interaction correction to Kohn-Sham orbital energies in order to apply ground state Khon-Sham DFT theory to accurate prediction of core electron binding energies and chemical shift [90]. We concern about surface systems within DFT frame. From the other point of view, in periodic calculations only valence electrons are considered to reduce the computational effort and it is not easy to get core electron orbital energies. So, it is improper to apply this method to our systems.

Complete screening picture

In the complete screening picture for calculating the binding energy, the ionization potential (IP) of core or valence levels are calculated as the energy difference between the optimized N-1 electron system and the neutral ground state[91], which is written as:

$$IP_k = E_{opt}|_{n_k=0} - E_{opt}|_{n_k=1} \tag{4.18}$$

This procedure largely improves the results with respect to the frozen orbital approximation.

If the core-ionized atom Z^* is replaced by the next element in the periodic table we have the (Z+1)- or equivalent core approximation[92, 93]. This method can be used not only for cluster type calculations but also for periodic calculations. As for applications, this method has been widely used to study the surface or interface core level shift of complex metallic systems[94–96] or for molecules chemisorbed on metals. We have successfully applied this method to study water-TiO_2 surfaces. Though the absolute binding energy can not be achieved, it can give good results for core level shift of atoms in different chemical environments.

Table 4.1: *C1s, N 1s and O 1s binding energies for Alanine: $CH_3CH(NH_2)COOH$.*

core level	exp.(eV)	Δ(eV)	Ref. [97](eV)	Δ(eV)	periodic Δ(eV)
C 1s	291.0	0.0	291.5-291.8	0.0-0.0	0.0-0.0
	292.2	1.2	293.0-293.3	1.5-1.5	1.2-1.3
	295.0	4.0	296.5-296.1	5.0-4.3	3.7-3.3
N 1s	405.2	0.0	405.4(I)	0.0	0.0
	405.9	0.7	406.3(IIa)	0.9	0.9
O 1s	538.2	0.0	538.0-537.3	0.0-0.0-0.7	0.0-0.0-0.9
	540.0	1.8	539.9-539.0	1.9-1.7-0.9	2.1-1.5-0.6

In periodic calculations, PAW method permits to change the core orbital occupations, and then new pseudopotential is generated for a core ionized state[98]. Within this frame, the occupation of core levels can also be set as fractional numbers and thus transition potential (TP)(0.5 occupation at core level) procedure can also be realized. The CLS of different chemical bonded atom in one molecule are calculated by PAW method with plane wave basis sets. Because the plane wave basis can better cover the space within the supercell, the calculations give better results than regular DFT cluster calculation for alanine. By this method, the binding energy of C 1s of COOH is underestimated. This information can be

obtained from isolated molecular calculations and is helpful to assign the attribution in complicated systems. The results of an example calculations for alanine are listed in Table 4.1

In high resolution XPS experiments, a series of weak satellites can be observed at the higher binding energy side of the XPS main lines. These satellites are usually denoted as XPS shake-up satellites, which result from the simultaneous core electrons ionization and the valence electrons excitation. Brena et al. have proposed equivalent core hole time-dependent density functional theory (ECH-TDDFT) [99, 100], which can be used in small systems. While for large systems, by noticing that the dominated excitation in shake-up is often from one particular excitation channel, Gao *et al.* speculate that there is only a single excitation for each final state, which can be determined by the orbital-orbital transition from the equivalent core hole Kohn-Sham (ECH-KS) density functional theory approach[101]. The shake-up phenomena is, however, out of the scope of this thesis.

4.1.2 Dynamic XPS spectra

According to the ergodic hypothesis in MD simulations, if the binding energy of a specific atom is calculated for a series of configurations during the equilibrium simulation, the XPS spectra, neglecting shake-up process, can be well reproduced. We can choose several snapshots along the MD trajectory and get bar diagrams at each configuration. By broadening the discrete binding energies, a spectrum quite similar to the experimental one can be obtained, which is named as dynamic XPS spectrum. This method has been applied to the simulation of the XPS spectra of water-rutile and anatase TiO_2 surfaces in **Paper VI** and **Paper VIII**. In Figure 4.2, the separate spectrum at different time are indicated to show the evolution of XPS spectra.

4.1.3 Hydrogen bond effects and vibrational effect

-OH, H_2O, -NH_2, -COOH etc. groups can form intramolecular or intermolecular hydrogen bond (H-bond) between each other. The H-bond effect can separate the O 1s binding energy oxygen in donor and acceptor groups by more than 1 eV, which has been verified by experiment and theoretical calculations of a number of amino acids including alanine and threonine[102]. The same effect is observed when phenylalanine, tyrosine and tryptophan are investigated. Interestingly, a phase transition is observed on water covered Anatase TiO_2 surface [103], by quantum

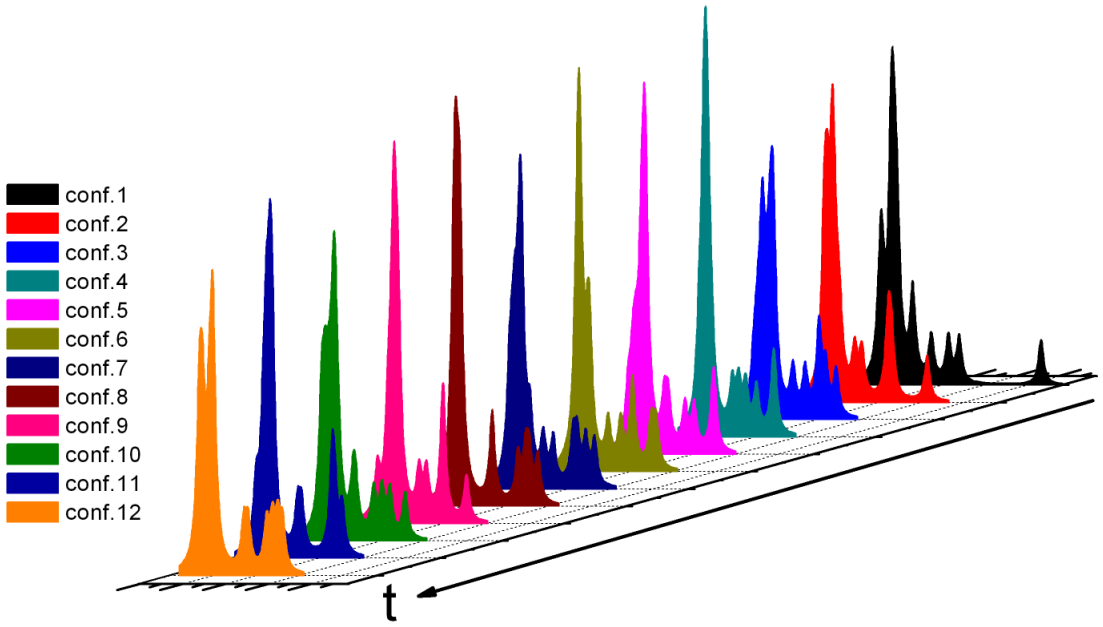

Figure 4.2: *Calculated O_{1s} photoemission spectra of adsorbate $H_2O/TiO_2(110)$ for 12 configurations taken out from the last 0.25 ps of the molecular dynamics simulation with equal time step. The main peak corresponds to the lowest binding energy. The continuous profile was obtained by a Lorentzian convolution with full width half maximum (FWHM) of 0.3 eV.*

mechanic MD simulations, which is induced by the formation and breakdown of hydrogen bonds(**Paper VIII**).

It is also found that in order to well interpret the intensities of each peak in Phenylalanine XPS spectra, the different contributions of different configurations at the experimental temperature, induced by vibrational effects, have to be considered.

4.2 X-ray absorption spectra

The near edge X-ray absorption fine structure (NEXAS) technique was developed in the 1980s with the goal of elucidating the structure of molecules bonded to surfaces, in particular low-Z (carbon, nitrogen and oxygen) molecules. NEXAFS selects a specific atomic species through its K-edge and probes its bonds to intramolecular, and to a lesser degree extra-molecular (i.e. surface atoms) neighbors. Among the capabilities are: the ability to detect the presence of specific bonds in molecules (e.g., C-C, C=C, C≡C and C-H bonds in hydrocarbonds), the de-

termination of the lengths of these intra-molecular bonds and the derivation of the precise orientation of molecules and functional groups on surfaces or solids. By comparison of spectra for free and chemisorbed molecules NEXAFS can also reveal which orbitals are involved in the chemisorption bond. To first order it gives no information on the detailed atomic adsorbate-substrate registry. This part of the problem can, however, be solved with the related and complementary surface extended X-ray absorption fine structure (SEXAFS) technique.

The transition element $\langle \Phi_f | r | \Phi_i \rangle$ is subject to a strict set of "atom-like" selection rules $\Delta l = \pm 1, \Delta s = \Delta j = 0, \pm 1, \Delta m_j = 0, \pm 1$(if $j = 0$, the transition $m_j = 0 \rightarrow m_j = 0$ is forbidden). For K-shell excitations (for instance O 1s), only transitions to p orbitals are allowed. More specially, due to the spatial localization of the O 1s orbital, only final state orbitals with a local p-character on the excited atom will have non-zero probability. Clearly, the spectrum will thus be dominated by the presence of O 2p orbitals on the excited atom. For linearly polarized photons (e.g. synchrotron radiation), the polarization dependent angular anisotropy makes XAS a valuable tool to determine average molecular orientations in ordered systems.

4.2.1 Theoretical method

The transition energy (for instance a 1 $s \rightarrow \pi^*$ excitation)is defined as:

$$\Delta E_k = E_{opt}|_{n_{1s}=0, n_{\pi^*}=1} - E_{opt}|_{n_{1s}=1, n_{\pi^*}=0} \tag{4.19}$$

which is named as ΔKS approach within DFT framework. But evidently, it is too complicated to calculate all the possible transitions, especially the transition to continuum states. To avoid such complex calculations, some methods have been developed to get the whole spectra by one or two calculations. One of which is named as Static Exchange approximation (STEX)[104–106] implemented in HF-SCF and DFT framework. The calculation of the absorption spectrum follows successive steps. The initial state is the calculation of the system's ground state. To determine the final state, first a fully relaxed optimization of the core hole state is performed, with the valence orbitals frozen, followed by a valence orbital calculation with the core hole frozen. Finally, by diagonalizing the STEX Hamiltonian, that describes the motion of the excited electron in the static field of the ion, the excited orbitals are generated, so that the excited state orbitals are orthonormal with respect to the relaxed core hole orbitals. The excitation energies are obtained by summing the core IP to the eigenvalues of the STEX Hamiltonian. The oscillator strengths are calculated from the dipole matrix between the ground and the final STEX states.

Based on the transition potential (TP) concept[91], a similar method to generate absorption spectra was implemented at the DFT level. Also the TP method allows to overcome the problem of calculating all excitation energies by the ΔKS method. The IP E_b(k) of the k-th orbital in the TP approximation can be expressed as the derivative of the total energy E_0 with respect to the orbital occupation number n_k. To take into account the relaxation, the IP can be approximated by calculating the derivative at the point corresponding to the occupation number $n_k = 0.5$,

$$E_b(k) = -\frac{\partial E_0(n_k)}{\partial n_k}|_{n_k=0.5}, \tag{4.20}$$

The procedure can also be carried out by choosing the occupation number $n_k = 0$ which is referred to as the full core hole (FCH) potential method. The full core hole effect becomes important to generate accurate NEXAFS spectra for fullerene molecules[107].

In the TP method, the initial and final states are computed in a single KS calculation with a double basis set technique. During the calculation, the molecular wave function is firstly optimized by a normal orbital basis set, and is later augmented by a larger diffuse basis set on the core excited atom in order to obtain a proper representation of the relaxation effect. The oscillator strengths are derived from the dipole matrix of the set of orthogonal vectors obtained. The transition energies are computed by summing the IP to the set of KS eigenvalues. To simulate the continuum part of the NEXAFS spectrum, a Stieltjes imaging technique[108, 109] is used above the IP.

In practice, the calculated NEXAFS spectra from the TP mothod are usually calibrated by the ΔKS calculations: the first spectral feature corresponding to the transition from the 1s level to the lowest unoccupied molecular orbital (LUMO) is made to coincide with the same one obtained from the Δ KS scheme where the energy is taken as the difference between the ground state and the fully optimized core-excited state. This method has been applied to some amino acids for instances phenylalanine, tyrosine and tryptophan.

5

Applications

5.1 Surface chemistry on Au(111)

To understand the versatility of surface chemistry on gold, it is important to investigate the adsorption properties of different molecules and intermediates. Au(111) surface exhibits a ABCABC$\cdots$ manner of close-packing and the outmost layer is supposed as A without loss of generality, by taking translation invariant of the surface into account. Usually, the adsorption at high symmetry sites are considered, such as fcc, hcp, bridge and atop site, where fcc (hcp) means the adsorbed atom locate at the hollows above C(B) layer; atop site represents adsorbates on the A layer atom and regarding bridge site the adsorbed atom binds to two surface atoms.

5.1.1 O_2 and O

Bulk gold does not easily adsorb or dissociate molecular oxygen, which can be verified by the low adsorption energy of 0.04 eV, calculated by DFT as $E_{ads} = E_{molecule} + E_{substrate} - E_{adsorbed}$. However, it does readily chemisorb oxygen in its atomic form when Au is exposed to O_3 or physisorbed oxygen is dissociated on Au surface at low temperature via electron bombardment[110, 111]. In **Paper I**, **II** the adsorption of atomic oxygen is investigated. Our results suggested that atomic oxygen prefers to adsorb at fcc hollow site and the adsorption energy decreases with the increasing of oxygen coverage. At 0.11 monolayer(ML) coverage, the adsorption energy of oxygen on Au(111) surface is 3.38 (2.69) eV [1], which is lower than the

[1]The numbers are from VASP and DMol^3, respectively. The difference comes from the energy of isolated oxygen atom.

value on other transition metal surfaces, for instance, 3.61 for Ag(111)[112], 5.03 for Cu(111)[113], 4.39 for Pt(111)[113].

5.1.2 NO and CO

Table 5.1: *The adsorption energy and geometrical parameters for NO and CO adsorption at different sites on clean Au(111) surface. θ is the angle between X-O molecular axis and the normal of the surface. The vibrational frequency of the gas phase XO is also listed. X indicates "C" or "N".*

molecule	structure	E_{ads}(eV)	d_{X-O} (Å)	d_{X-Au} (Å)	θ	fre(cm^{-1})
NO	fcc	0.28	1.19	2.33	∼0°	1618
	hcp	0.22	1.19	2.38	∼0°	1646
	atop	0.41	1.17	2.22	∼38°	1757
CO	fcc	0.14	1.17	2.23	∼0°	1837
	hcp	0.11	1.17	2.25	∼0°	1846
	atop	0.25	1.14	2.02	∼0°	2084

The adsorption of NO and CO are investigated in **Paper I** and **Paper II**, respectively. NO and CO both prefer to adsorb at atop site, while, the geometries are different: NO has a tilt geometry, in which the N-O axis tilts away from the normal direction of 38°; while, CO stands upright on the surface as the adsorption at other sites. The adsorption of NO is a bit stronger than that of CO. This difference may be a result of the half occupied high occupied molecular orbital (HOMO) of NO, which is more ready to bounding with other atoms.

5.1.3 NO/CO oxidation on O/Au(111) surface

Mullins *et al.*[114] found that NO may react with chemisorbed oxygen (∼ 0.95 ML coverage) atoms at temperature as low as $T_s \sim 85K$. In **Paper I**, the NO oxidation processes on oxygen covered Au(111) surfaces with 0.33 ML and 1.0 ML coverage are investigated. The reaction barriers of all elementary steps are studied with drag-method and summarized as:

At moderate (0.33 ML) coverage

$$NO(g) + O_{ads} \longrightarrow NO_2(chemisorbed) \qquad E_a < 0.18eV$$
$$NO_2(chemisorbed) \longrightarrow NO_2(gas) \qquad E_a = 0.64eV.$$

At high (1.0 ML) coverage

$$
\begin{aligned}
NO(g) + O_{ads} &\longrightarrow NO_2(physisorbed) && no \quad barrier \\
NO_2(physisorbed) &\longrightarrow NO_2(gas) && E_a = 0.03eV \\
&or \\
NO(g) + 2O_{ads} &\longrightarrow NO_3(chemisorbed) && no \quad barrier \\
NO_3(chemisorbed) &\longrightarrow NO_2(gas) + O_{ads} && E_a > 1.79eV.
\end{aligned}
$$

NO can react with precovered oxygen to $NO_{2,ads}$ by conquering small barriers on low(0.11 ML), moderate(0.33 ML), and high(1.0 ML) oxygen coverage Au(111) surfaces. On moderate oxygen coverage surface, NO reacts with precovered atomic oxygen to form chemisorbed NO_2 with a barrier of ∼0.18 eV and the desorption energy of NO_2 is 0.64 eV. However, this is not the case for reaction with high oxygen coverages, where there is no barrier for NO reaction with oxygen atom and an overall barrier of about 0.03 eV is found for NO_2 desorption. So the desorption of NO_2 is the rate-limiting step on moderate and high oxygen covered surface. The reactions proceed via E-R mechanism. On high oxygen coverage surface, NO can also react with two surface oxygen atoms to form chemisorbed NO_3 group, which will prohibit the production of NO_2.

Mullins *et al.* also found that CO can be oxidized on low coverage oxygen precovered Au(111) surfaces and the production of CO_2 increases with the presence of water[115]. For CO oxidation, a low oxygen coverage (0.11 ML) surface is adopted and H-L mechanism is suggested. Co-adsorbed CO and O react with each other to form CO_2(gas). The energy barrier of this elementary step is 0.39 eV, which is studied in **Paper II**.

5.1.4 H_2O, H_3O and OH

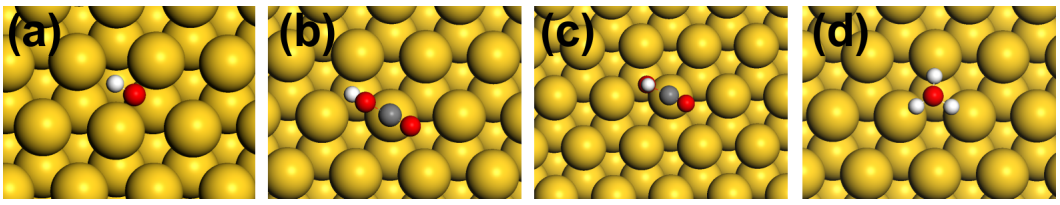

Figure 5.1: *Schematic structures of the surface-adsorbed OH(a),* trans-*HOCO(b),* cis-*HOCO(c), and OH_3(d). The gold atoms, oxygen atoms, carbon atoms and hydrogen atoms are represented by the yellow, red, gray and white spheres, respectively.*

When water adsorbs on the oxygen pre-covered surfaces, it can lose a hydrogen atom to be OH or gain a hydrogen atom to form H_3O. OH and H_3O will play an important role in CO oxidation. In **Paper II**, the adsorption of H_2O, H_3O and OH are investigated. Water molecule only weakly adsorbs on Au(111) surface with an adsorption energy of 0.11 eV, which permits water to freely rotate or diffuse on the surface. H_3O binds to the surface through three hydrogen atoms and it can be stabilized by oxygen, hydroxyl, or water on the surface. OH prefers to adsorb at bridge site, and the energy difference between each site is within 0.2 eV, which allows OH diffuse easily.

It is hard for water to dissociate on clean Au(111) surface. While with the present of precovered atomic oxygen atom, strong hydrogen bond is formed between each other, which permits water to dissociate to OH_{ads} with a energy barrier as low as 0.33 eV. OH_{ads} is a very important species during CO oxidation.

5.1.5 HOCO and the reaction of CO + OH

HOCO, the intermediate of reaction OH+CO, has two conformers: *trans*- and *cis*-, which binds the atop site through carbon atom. The structures of *trans*- and *cis*-HOCO are shown in Figure 5.1. *trans*-HOCO is about 0.05 eV more stable than *cis*-HOCO. The dissociation of HOCO generates gas phase CO_2 and H related surface groups, such as, OH, H_2O or H_3O. In my work, *trans*-HOCO is chosen as the intermediate. The energy barrier of CO+OH→ *trans*-HOCO is 0.44 eV. The crucial step is the dissociation of *trans*-HOCO. On water-oxygen/Au(111) surface, it can react with neighboring O_{ads} or OH_{ads} to give off CO_2(gas), while, such mechanisms do not generate more CO_2. Otherwise, it can react with close-by water molecule to dissociate to CO_2 and leave a H_3O on the surface. More CO_2 than only oxygen covered surface is produced on water-oxygen covered surfaces. This part of results are present in **Paper II**.

5.1.6 Diamondoid on gold/silver surface

Diamondoid, nanometer-sized diamond clusters saturated by hydrogen atoms, has attracted considerable attention because of its negative electron affinity (NEA). NEA materials have practical applications in cold cathode emitters, ultraviolet detectors, and field-emission devices (FEDs).

By attaching a -SH on diamondoid, it is easy to form self-assembled monolayers (SAMs) on noble metal surfaces, for example [121]tetramantane-6-thiol (TM-6-S). A single sharp low energy peak is observed in the photoemission spectroscopy

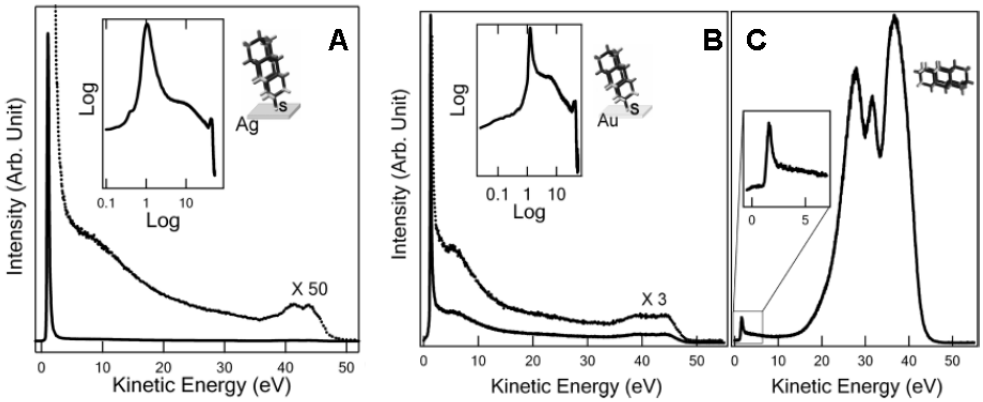

Figure 5.2: *(A) Photoelectron spectra of TM-6-S SAMs grown on Ag substrates. The sharp peak at 1 eV contains about 67% of the total photoelectrons. (B)Photoelectron spectra of TM-6-S SAMs grown on Au substrates. The sharp peak at 1 eV contains about 17% of the total photoelectrons. The inset shows a double logarithm plot. (C) Photoelectron spectra of TM films prepared in situ on Au substrates. The inset is an enlargement of the low−kinetic energy part of the spectrum showing only a small peak. Taken from Ref. [20].*

(PES)(as shown in Figure 5.2). While, there is only a weak peak for unsubstituted TM. -SH group dissociates to -S on metal surfaces. For comparison, the adsorption of unsubstituted diamondoid (TM) is also investigated. In **Paper III**, the adsorption of TM and TM-6-S on gold and silver surfaces are investigated and a possible mechanism of electron emission is suggested.

TM-6-S prefers to adsorb at fcc hollow site with a small polar angle. By ground state electronic structure calculations, it is found that the partial density of states (PDOS) is extended below the vacuum level in all the systems studied. A comparison between gold and silver adsorbed system, shows that the latter has the lower work function, which suggests that it is easier to generate much more efficient electron photoemission on silver surface. For TM-6-S, there is good chemical bonding between molecule and metal surfaces, while, the hybridization is very weak between TM and surface, which is indicated by almost zero gap states. The hybridization between molecule and silver surface is weaker than that of gold surface, which induces more localized unoccupied states to accumulate electrons in the second system. The ground state picture is in contract with the definition of NEA and can not explain the photoemission mechanism. Cluster calculations have shown that by exciting an electron in the lowest unoccupied molecular orbital, the highest singly occupied molecular orbital of the molecule shifts above the vacuum level, resulting in negative electron affinity and emission of the accumulated electrons.

5.1.7 BDT adsorption with different contact configuration

For its simplicity, benzene-1,4-dithiol molecule is usually used as a model system in molecular device studies. Theoretical studies have indicated that the structure of contact region is very important to get comparable results with experiments. In **Paper IV**, a BDT molecule adsorbed on gold surfaces, gold nanowire and gold clusters is investigated. It is suggested that a BDT molecule prefers to adsorb on the most irregular site of a gold surface. The higher adsorption energy structures do not necessarily cause higher conductivity. So in the theoretical studies on molecular device, it is important to ascertain exact contact structures. In addition, the S 1s XAS spectra for each contact structure are predicted, which show that X-ray spectroscopy could be a powerful method to study the structure of molecule-metal junctions.

5.2 Oxide surface

5.2.1 FeO ultrathin film

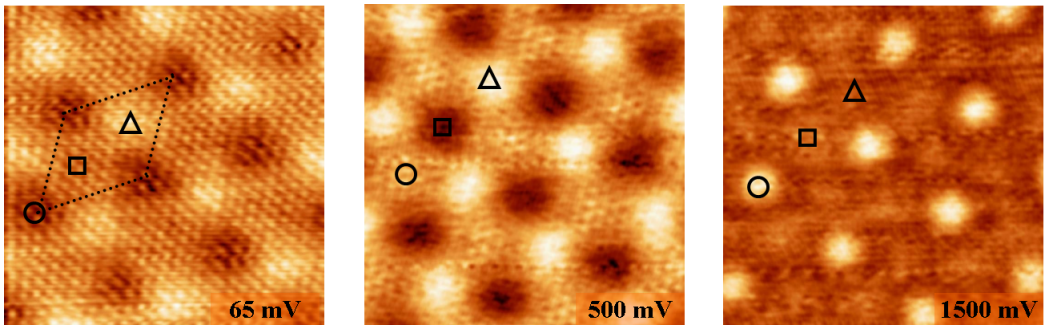

Figure 5.3: *STM topographic images of FeO on Pt(111) taken at the bias voltages indicated in the images. The symbols mark the different stacking domains within the FeO Moiré cell(Fe-top, circle; Fe-hcp, triangle; Fe-fcc, square). (a) Bias V=65 mV; (b) Bias V=500 mV; (c) Bias V= 1500 mV. Taken from Ref. [24]*

FeO/Pt(111) ultrathin film has potential application on catalysis and self-assembled monolayer (SAM). For the mismatch between FeO layer and Pt layer, the periodicity of FeO/Pt(111) is ∼26Å. The layer distance of iron and oxygen is 0.68 Å, which is an important parameter for this film. There are three special regions in the surface unit cell: the top region where Fe atoms grow right upon Pt atoms, the hcp where the lateral coordinates of Fe atoms are almost coincident with the

second layer of Pt atoms and oxygen atoms are located above the first layer Pt atoms, and the fcc region where both iron and oxygen atoms locate at hollow sites. Iron containing systems always have various magnetic structures. Ferromagnetic resonance (FMR) spectra indicate that the film does not exhibit ferromagnetic (FM) order. In tunneling spectra at low bias, the local density of states around the Fermi energy is featureless at most positions in the unit cell, however, a pronounced depression is observed at the top region. The STM images show contrast evolution when the bias increases from 65 to 1500 meV.

According to the observed experimental phenomena, different magnetic structures are supposed to simulate the properties of the ultrathin film in **Paper V**. By comparison, top-7 model (seven iron with opposite spin direction with others) is suggested as the best one to reproduce the experimental observations. The order of iron-oxygen layer (δ_z) is $\delta_z^{top} < \delta_z^{hcp} < \delta_z^{fcc}$, which is discovered for the first time and is very important to achieve a correct assignment of STM images. With top-7 model, the electronic structures of different local regions are simulated. The STM image at low bias is well reproduced. The local surface potential is calculated to explain the resonant tunneling of each region.

5.2.2 Water covered rutile TiO_2(110) surface

Among the experimental and theoretical investigations on several species adsorbed on TiO_2, those regarding the interaction between water and rutile (110) surface, have been predominant due to the fundamental role played by water in a large number of chemical and biological processes. Water is easy to dissociate on oxygen defect rutile (110) surface to form two OH. Nevertheless, the extent to which H_2O does dissociate to produce surface hydroxyl species on a clean and perfect TiO_2 surface remains a subject of controversy. In **Paper VI**, the adsorption of water on perfect TiO_2 surface is studied by quantum molecular dynamics simulation adopting a periodic model formed by five water molecules on a (5×1) surface unit cell. The total simulation time is 3.2 ps. At about 1.3 ps, one water molecule dissociates with the help of other adsorbed waters and surface bridging oxygens. During the remaining 1.9 ps, the waters and OH groups vibrate, but no more dissociation or recombination is observed except the temporary recombination near 1.6 ps and the short-lived donor acceptor switch. The average values for the Ti-O distances of the three adsorbed water molecules are 2.16, 2.24 and 2.22 Å. Averaged over all chemisorbed water molecules, the Ti-O distance is 2.21 Å, which agrees very well with the experimental results. The average bond length of Ti-O(OH) is

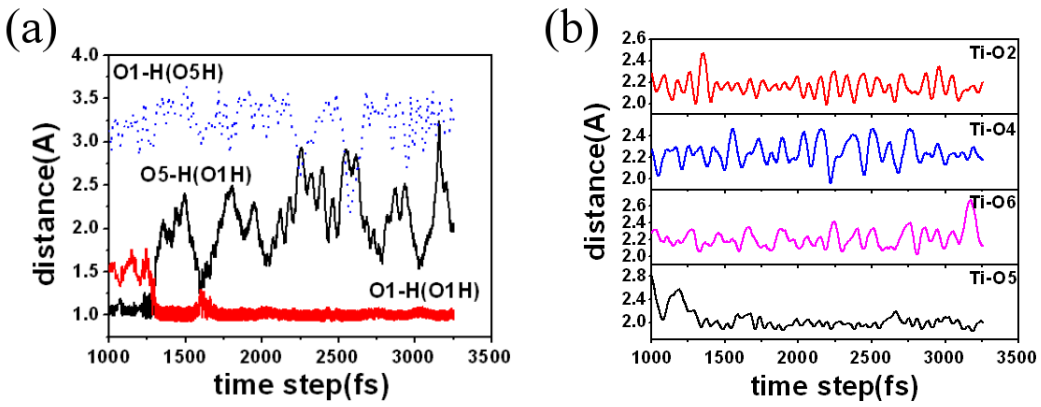

Figure 5.4: *Inter atomic distances O-H (a) and Ti-O (b) vs time during the last 2.2ps of the MD simulation.*

1.99 Å.

By comparing recent experimental O 1s photoemission spectra of $H_2O/TiO_2(110)$ to the computed spectrum of the adsorbate in the configurations supplied by the molecular dynamics simulation, the observed peaks can be attributed to different oxygen species. The proposed assignment of the main spectral features supports the occurrence of partial water dissociation (∼20%) also on a perfect TiO_2.

5.2.3 Phase transition of water/anatase(001) surface

Understanding the effects of water adsorption on anatase is of uttermost importance, as water is a required ingredient for several growth processes, and the presence of water is also common in the operating conditions of anatase-based devices, e.g. in dye-sensitized solar cells[116]. Sandell and his coworkers[33] measured the XPS spectra of water covered anatase $TiO_2(001)$-(4×1) reconstructed surface at various dose and temperature. The experimental spectra are shown in Figure 5.5. Three groups of peaks are observed during all the situations and they are assigned as surface oxygen, OH groups and oxygen of water, from low to high binding energies. Only two low binding energy peaks are observed at 190 K and low water coverage, which is labeled as phase 1. Moreover with the increasing of water coverage, all three peaks are observed. After careful analysis, it was found that the area of peak 2 is double of that in phase 1 and this high coverage phase is labeled as phase 2. When temperature increases above 230 K, phase 2 transits to phase 1. The experimentalists suggested that phase 1 arises from the dissociation of water on ridge, but the structure of the high coverage phase is at present unclear.

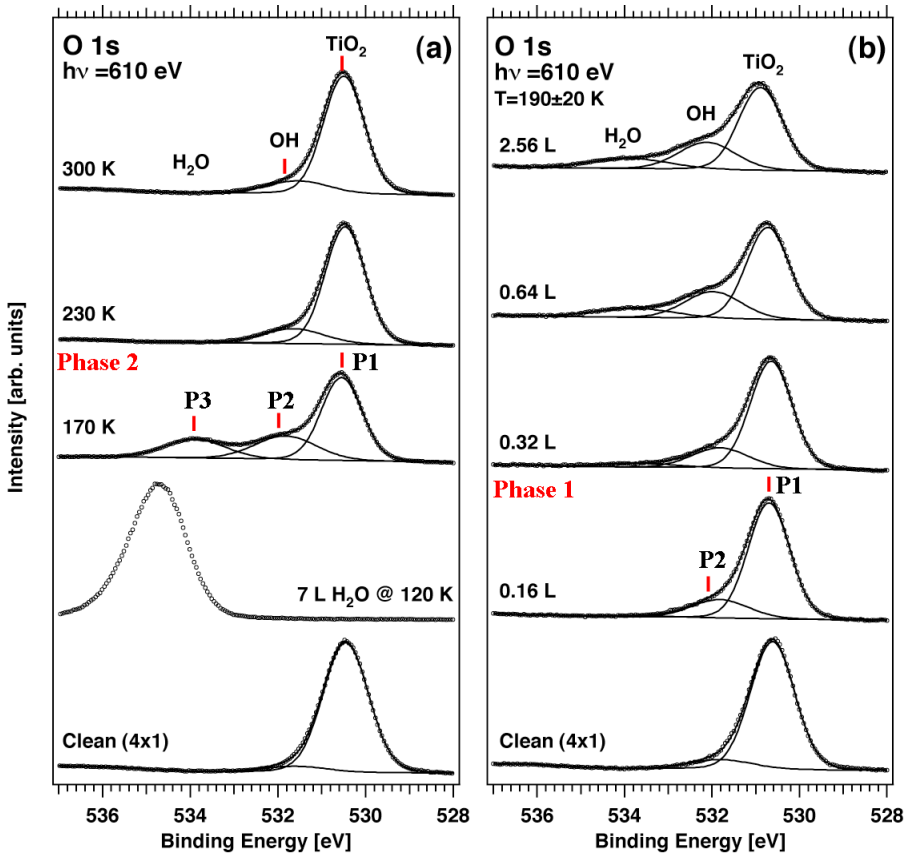

Figure 5.5: *O 1s core level photoemission spectra for water adsorbed on anatase TiO_2(001)-(4×1): (a) Heating of a multilayer of water. (b) Progressive adsorption at low temperature. From Ref. [33]. The two phases and three peaks are labeled in the figure.*

In **Paper VIII**, by quantum molecular dynamics simulations of water covered perfect and reconstructed anatase TiO_2(110) surfaces with (4×2) surface unit, it is found that hydrogen bonds between water-hydroxyl, hydroxyl-hydroxyl, and water-water play important roles to explain experimental observations. On reconstructed surface, one water molecule dissociates at ridge to form two hydroxyls: one is donor (OH_D) and the other is acceptor (OH_A). The binding energy of O 1s in OH_A corresponds to peak 2, which is assigned to OH group by the experimentalists; while the O 1s binding energy of OH_D is very close to that of the surface oxygen atoms. When only OH is present on surface, only Peak 1 and Peak 2 are observed, and the ratio of Peak 2 and Peak 1 is about 0.2. At high water coverage, no more waters dissociate on the surface, while the peak of OH group is doubled and a water peak is present, which is attributed to the $HO_D \cdots H_2O$ hydrogen bond that pushes the binding energy of the OH_D to higher energy value.

This effect is also observed in XPS investigations of amino acids (phenylalanine, tyrosine, tryptophan).

5.2.4 Graphene oxide and cut mechanism

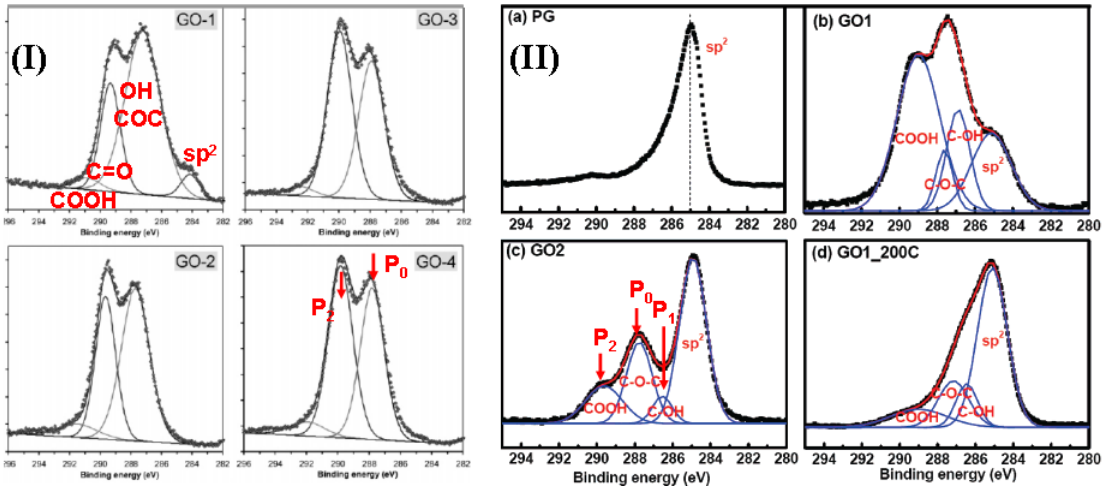

Figure 5.6: *(I) and (II) Experimental XPS spectra from Ref. [47] and [46], respectively.*

The structure of graphene oxide (GO) has been intensively studied by experiments and first principle calculations. Several measurements have been performed to investigate the structure of GO, for example, X-ray diffraction(XRD) to get the layer distance after oxidation, ^{13}C magic-angel spinning NMR, X-ray photoelectron spectroscopy (XPS), X-ray absorption spectroscopy (XAS), electron spin resonance (EPR) and so on. Still, the structure of GO is largely unclear. In principle, the species possibly present on GO sheet are: epoxide, hydroxyl, carboxyl and even carbonyl groups. NMR measurements suggest that carbonyl groups may be mostly distributed at the edge of GO and thus closely related to the oxidation induced graphene break-up process. Experimental XPS studies of GO have provided more detailed structure information[46, 47], but their structure assignments differ greatly from one group to another.

In **Paper IX**, relative core chemical shift (R-CCS) of carbon atoms in different oxidation species are calculated using density functional theory. The calculated results are collected in Table 5.2, together with the experimental results for comparison. Our calculations have given clear assignments for experimental XPS spectra. We have found that several previous suggested assignments based on experimental spectra alone are not correct. The importance of theoretical calculations for un-

Table 5.2: *Experimental and calculated relative core chemical shift (R-CCS) of C1s for different oxidation species on GO. The experimental results are reassigned following the theoretical characterizations. The binding energy of C-epoxide at 287.2 eV is set to be the common reference point for all theoretical and experimental results.*

	Periodic.	cluster	Ref. [47]	Ref. [46]
C-H	-2.6			
C-C	-2.4 - -1.5	-2.0	-3.1	-2.2 (±1.2)
CH_3	-1.4			
C-OH-edge	-0.8			-0.8 (±1.0)[c]
C=O-edge	-0.9	-0.5		-0.8 (±1.0)
C-OH-inner	+0.0	+0.1	0.0 (±1.2)	
C-epoxide	0.0	0.0	0.0 (±1.2)	0.0 (±1.0)
C=O-inner		+0.1		
C-EP	+0.8 - +0.9	+1.1	+2.1 (±1.2)	+1.8 (±1.2)[d]
COOH	+1.2	+1.7	+2.1(±1.2) [a]	+1.8 (±1.2)
COOO	+3.2		+3.6(±1.0) [b]	

[a] and [b] were assigned to carbonyl and carboxyl, respectively[47].
[c] and [d] were assigned to C-OH group and carboxyl, respectively[46]

derstanding chemical and electronic structures of GO is thus well illustrated. The new structure information revealed by XPS calculations has helped us to build a new model to study cleavage mechanism for graphene oxide sheet.

In Paper **X**, possible cut mechanisms of graphene oxide sheet are investigated, which is valuable for developing effective graphene manipulation means and for understanding the long puzzling GO structure. Our results suggest that a well controlled oxidation induced cut of graphene could lead to more smooth edges compared to heat or sonic treatment. Our first principles calculations reveal that oxidative cut of graphene is realized by forming epoxy and then carbonyl pairs. On an epoxide chain, the energy barrier for the epoxide pair is 0.76 eV, while the barrier for the neighboring epoxide pair is dramatically reduced to 0.26 eV. We have found that direct forming carbonyl pair to tear graphene up from an edge position is not favorable in energy.

6

Future outlook

"Little by little one goes far."

6.1 Catalysis

Heterogeneous catalysis has important application in modern industry, which includes catalysts for pollution and emission control, chemical processing of bulk and specially chemical, clean hydrogen production for the emerging 'hydrogen economy' and fuel cells and sensors to detect poisonous or flammable gases or substances in solution. Those involved in investigating the development of various applications are making progress towards viable methods of manufacturing significant quantities of catalyst and devising reliable preparative methods for ensuring suitable durability of catalysts under required operating conditions.

There are many important chemical processes deserving carefully investigations. Theoretical calculations may help to understand the reaction mechanism and maybe help to design catalyst. In this thesis, the emphasis is put on gold catalysis and we have studied the oxidation of NO and CO on atomic oxygen covered Au (111) surface, which are basic surface reactions. In the future, we would like to investigate more processes related to gold surface or gold nanoparticles, such as the oxidation of methanol, propanol, propylamine etc. [117–119] on O/Au(111) surface. And also we are interested at the chemical processes at different reaction conditions. Another field of interest is the catalysis process on gold alloy for example, the oxidation of CO Au/Ni surface[120]. We hope we can predict some special catalysis some day to help improving the activity.

6.2 Combined spectroscopies with surface investigations

Electron and photon spectroscopies are widely used to determine the surface structure and properties of catalyst and surfaces. In this thesis, with periodic calculations, the vibrational frequencies of adsorbed species are calculated to compare with the experimental results and also the relative binding energies of atoms in different chemical environments are obtained to help to determine the surface structures. Periodic calculations can offer more lateral interaction information, but sometimes, if the lateral interaction is not so important, it will be expensive and less accurate. Some spectroscopies are still challenges for periodic calculations; so, it is necessary to utilize both cluster and periodic calculations.

Firstly, we want to calculate the XAS spectra with slab models to consider the interaction between adsorbates. Recently, this kind of calculations have been applied to study the X-ray absorption spectra of diamond[57], graphite[56], nanotube, graphene and liquid water[53–55] systems. Some groups have implemented the algorithm in different codes (VASP, GPAW and so on). One of them is reciprocal-space pseudopotential scheme, which incorporates a recursive method to compute absorption cross section as a continued fraction. The continued fraction formulation of absorption is advantageous in that it permits the treatment of core-hole interaction through large supercells (hundreds of atoms). The method can be compared with recently developed Bethe-Salpeter approach. The method was applied to the carbon K edge in diamond and to the silicon and oxygen K edges in $\alpha-$quartz for which polarized NEXAFS spectra were measured. Core-hole effects are investigated by varying the size of the supercell, thus leading to information similar to that obtained from cluster size analysis usually performed by multiple scattering calculations[57].

Quantum chemistry has provided many methods to simulate the spectroscopies, IR, NMR, Raman and so on. It is crucial to build reasonable models for cluster calculations. For metal surfaces, it is relatively easy for the special properties of metals, while for oxide surfaces, point charges have to be used to simulate the interaction of surrounding ions.

Until now, most of my works have been performed by the periodic scheme, but, molecular investigations played an important role to understand the physical and chemical observations. In the future, I would like to learn some skills of cluster calculations and hope both periodic and cluster calculations can well promote each other.

References

[1] M. Haruta, Catal. Today, **36**, 153, 1997.

[2] M. Haruta, S. Tsubota, T. Kobayashi, H. Kageyama, M. J. Genet, and B. Delmon, J. Catal., **144**, 175, 1993.

[3] M. Okumura, S. Tsubota, and M. Haruta, J. Molec. Catal. A: Chem, **199**, 73, 2003.

[4] M. Valden, X. Lai, and D. W. Goodman, Science, **281**, 1647, 1998.

[5] W. Liu and M. Flytzani-Stephanopoulos, J. Catal., **153**, 304, 2002.

[6] P. Bera and M. S. Hegde, Catal. Lett., **79**, 75, 2002.

[7] S. Arii, F. Mortin, A. J. Renouprez, and J. L. Rousset, J. Am. Chem. Soc., **126**, 1199, 2004.

[8] J. D. Grunwaldt, M. Maciejewski, O. S. Becker, P. Fabrizioli, and A. Baiker, J. Catal., **186**, 458, 1999.

[9] D. A. H. Cunningham, W. Vogel, and M. Haruta, Catal. Lett., **63**, 43, 1999.

[10] J. Guzman and B. C. Gates, J. Am. Chem. Soc., **126**, 2672, 2004.

[11] H. H. Kung, M. C. Kung, and C. K. Costello, J. Catal., **216**, 425, 2003.

[12] C. K. Costello, J. Guzman, J. H. Yang, Y. M. Wang, M. C. Kung, B. C. Gates, and H. H. Kung, J. Phys. Chem. B, **108**, 12529, 2004.

[13] R. B. Pontes, F. D. Novaes, A. Fazzio, and A. J. R. Silva, J. Am. Chem. Soc., **128**, 8996, 2006.

[14] M. A. Reed, C. Zhou, C. J. Muller, T. P. Burgin, and J. M. Tour, Science, **278**, 252, 1997.

[15] J. Jiang, M. Kula, and Y. Luo, J. Chem. Phys., **124**, 034708, 2006.

[16] X. Xiao, B. Xu, and N. J. Tao, Nano Lett., **4**, 267, 2004.

[17] P. Maksymovych and J. T. Y. Jr., J. Am. Chem. Soc., **130**, 7518, 2008.

[18] N. D. Drummond, Nature Mater., **2**, 462, 2007.

[19] N. D. Drummond, A. J. Williamson, R. J. Needs, and G. Galli, Phys. Rev. Lett., **95**, 096801, 2005.

[20] W. L. Yang, J. D. Fabbri, T. M. Willey, J. R. I. Lee, J. E. Dahl, R. M. K. Carlson, P. R. Schreiner, A. A. Fokin, B. A. Tkachenko, N. A. Fokina, W. Meevasana, N. Mannella, K. Tanaka, X. J. Zhou, T. van Buuren, M. A. Kelly, Z. Hussain, N. A. Melosh, and Z. X. Shen, Science, **316**, 1460, 2007.

[21] Y. Wang, E. Kioupakis, X. Lu, D. Wegner, R. Yamachika, J. E. Dahl, R. M. K. Carlson, S. G. Louie, and M. F. Crommie, Nature Mater., **7**, 38, 2008.

[22] W. A. Clay, Z. Liu, W. Yang, J. D. Fabbri, J. E. Dahl, R. M. K. Carlson, Y. Sun, P. A. Pianetta, and Z. Shen, Nano. Lett., **9**, 57, 2009.

[23] M. Date, M. Okumura, S. Tsubota, and M. Haruta, Angew. Chem. Int. Ed., **43**, 2129–2132, 2004.

[24] L. Giordano, G. Pacchioni, J. Goniakowski, N. Nilius, E. D. L. Rienks, and H. J. Freund, Phys. Rev. B, **76**, 075416, 2007.

[25] E. D. L. Rienks, N. Nilius, L. Giordano, J. Ganiakowski, G. Pacchioni, M. P. Felicissimo, T. Risse, H. P. Rust, and H. J. Freund, Phys. Rev. B, **75**, 205443, 2007.

[26] L. R. Merte, J. Knudsen, L. C. Grabow, R. T. Vang, E. Lægsgaard, M. Mavrikakis, and F. Besenbacher, Surf. Sci., **603**, L15, 2009.

[27] W. X. Huang and W. Ranke, Surf. Sci., **600**, 793, 2006.

[28] D. Diebold, Surf. Sci. Rep., **48**, 53, 2003.

[29] H. Perron, J. Vandenborre, C. Domain, R. Drot, J. Roques, E. Simoni, J. J. Ehrhardt, and H. Cataletter, Surf. Sci., **601**, 518, 2007.

[30] G. Ketteler, S. Yamamoto, H. Bluhm, K. Andersson, D. E. Starr, D. F. Ogletree, H. Ogasawara, A. Nilsson, and M. Salmeron, J. Phys. Chem. C, **111**, 8278, 2007.

[31] I. M. Brookes, C. A. Muryn, and G. Thornton, Phys. Rev. Lett., **87**, 266103, 2001.

[32] S. Wendt, J. Matthiesen, R. Cshaub, E. K. Vestergaard, E. Laegsgaard, F. Besenbacher, and B. Hammer, Phys. Rev. Lett., **96**, 066107, 2006.

[33] J. Blomquist, L. E. Walle, P. Uvdal, A. Borg, and A. Sandell, J. Phys. Chem. C, **112**, 16616, 2008.

[34] A. Vittadini, A. Selloni, F. P. Rotzinger, and M. Grätzel, Phys. Rev. Lett., **81**, 2954, 1998.

[35] G. S. Herman, M. R. Sievers, and Y. Gao, Phys. Rev. Lett., **84**, 3354, 2000.

[36] X. Q. Gong, A. Selloni, M. Batzill, and U. Diebold, Nature. Mat., **5**, 665, 2006.

[37] M. Lazzeri and A. Selloni, Phys. Rev. Lett., **87**, 266105, 2001.

[38] X. Q. Gong, A. Selloni, and A. Vittadini, J. Phys. Chem. B, **110**, 2804, 2006.

[39] S. Stankovich, D. A. Dikin, G. H. B. Dommett, K. M. Kohlhaas, E. J. Zimney, E. A. Stach, R. D. Piner, S. T. Nguen, and R. S. Ruoff, Nature, **442**, 282, 2006.

[40] P. M. Ajayan and B. I. Yakobson, Nature, **441**, 818, 2006.

[41] D. A. Dikin, S. Stankovich, E. J. Zimney, R. D. Piner, G. H. B. Dommett, G. Evmenenko, S. T. Nguyen, and R. S. Ruoff, Nature, **448**, 457, 2007.

[42] D. Li and R. B. Kaner, Science, **320**, 1170, 2008.

[43] Y. Dzenis, Science, **319**, 419, 2008.

[44] X. L. Li, X. R. Wang, L. Zhang, S. Lee, and H. J. Dai, Science, **319**, 1229, 2008.

[45] J. L. Li, K. N. Kudin, M. J. McAllister, R. K. Prud'homme, I. A. Aksay, and R. Car, Phys. Rev. Lett., **96**, 176101, 2006.

[46] H. K. Jeong, Y. P. Lee, R. J. W. E. Lahaye, M. H. Park, K. H. An, I. J. Kim, C. W. Yang, C. Y. P. R. S. Ruoff, and Y. H. Lee, J. Am. Chem. Soc., **130**, 1362, 2008.

[47] T. Szabó, O. Berkesi, P. Forgó, K. Josepovits, Y. Sanakis, D. Petridis, and I. Dékány, Chem. Mater., **18**, 2740, 2006.

[48] D. Briggs(ed.). *Handbook of X-Ray and Ultraviolet Photoelectron Spectroscopy.* Heyden, London, 1978.

[49] P. Ghosh. *Introduction to Photoelectron Spectroscopy.* Wiley, New York, 1983.

[50] T. Barr. *Modern ESCA: The Principles and Practice of X-Ray Photoelectron Spectroscopy.* CRC Press, Boca Raton, FL, 1994.

[51] J. F. Watts and J. Wolstenholme. *An Introduction to Surface Analysis by XPS and AES.* Wiley, Chichester, 2003.

[52] A. M. Venezia, Catal. Today, **77**.

[53] D. Prendergast and G. Galli, Phys. Rev. Lett., **96**, 215502, 2006.

[54] B. Hetényi, F. D. Angelis, P. Giannozzi, and R. Car, J. Chem. Phys., **120**, 8632, 2004.

[55] M. Cavalleri, M. Odelius, D. Nordlund, A. Nilsson, and L. G. M. Pettersson, Phys. Chem. Chem. Phys., **7**, 2854, 2005.

[56] P. A. Brühwiler, A. J. Maxwell, C. Puglia, A. Nilsson, S. Andersson, and N. Mårtensson, Phys. Rev. Lett., **74**, 614, 1995.

[57] M. Taillefumier, D. Cabaret, A. M. Flank, and F. Mauri, Phys. Rev. B, **66**, 195107, 2002.

[58] P. Hohenberg and W. Kohn, Phys. Rev., **136**(3B), B864–B871, Nov 1964.

[59] W. Kohn and L. J. Sham, Phys. Rev., **140**(4A), A1133–A1138, Nov 1965.

[60] G. Tu, V. Carravetta, O. Vahtras, and H. Agren, J. Chem. Phys., **127**, 174110, 2007.

[61] S. H. Vosko, L. Wilk, and M. Nusair, J. Phys., **58**, 1200, 1980.

[62] J. P. Perdew and Y. Wang, Phys. Rev. B, **45**, 13244, 1992.

[63] A. D. Becke, Phys. Rev. A, **38**, 3098, 1988.

[64] J. P. Perdew and K. Burke, J. Quant. Chem., **57**, 767, 1996.

[65] V. I. Anisimov, F. Aryasetiawan, and A. I. Lichtenstein, J. Phys.: Condensed Matter, **9**, 767–808, 1997.

[66] V. I. Anisimov, J. Zaanen, and O. K. Andersen, Phys. Rev. B, **44**, 943, 1991.

[67] J. Hubbard, Proc. Roy. Soc. London, series A, **285**, 542, 1965.

[68] S. L. Dudarev, G. A. Botton, S. Y. Savrasov, G. J. Humphreys, and A. P. Sutton, Phys. Rev. B, **57**, 1505, 1998.

[69] M. R. Norman, Phys. Rev. B, **40**, 10632–10634, 1989.

[70] G. Kresse and J. Hafner, Phys. Rev. B, **47**, 558, 1993.

[71] G. Kresse and J. Hafner, Phys. Rev. B, **48**, 13115, 1993.

[72] G. Kresse and J. Hafner, Phys. Rev. B, **49**, 14251, 1994.

[73] G. Kresse and J. Joubert, Phys. Rev. B, **59**, 1758, 1999.

[74] B. Hetényi, F. D. Angelis, P. Giannozzi, and R. Car, J. Chem. Phys., **115**, 5791, 2001.

[75] D. Vanderbilt, Phys. Rev. B, **41**, 7892, 1990.

[76] G. Kresse and D. Joubert, Phys. Rev. B, **59**, 1758, 1999.

[77] C. Bai. *Scanning tunneling microscopy and its application.* Springer Verlag, 2nd edition, New York, 1999.

[78] J. Tersoff and D. R. Hamann, Phys. Rev. B, **31**, 805, 1985.

[79] C. L. G. C. Bond and D. T. Thompson. *Catalysis by Gold.* Imperial College Press, 2006.

[80] G. Henkelman, G. Jóhannesson, and H. Jósson. *Progess on Theoretical Chemistry and Physics.* edited by S. D. Schwartz(Kluwar, Dordrecht), 2000.

[81] T. A. Halgren and W. N. Lipscomb, Chem. Phys. Lett., **49**, 225, 1997.

[82] M. J. Rothman and L. L. Lohr, Chem. Phys. Lett., **70**, 405, 1980.

[83] T. A. Halgren and W. N. Lipscomb, Chem. Phys. Lett., **49**, 225, 1977.

[84] P. Gava. *Modeling the catalyst selectivity in the ethylene epoxidation reaction—A first principles study.* PhD thesis, 2005.

[85] R. L. Cropley, F. J. Williams, O. P. H. Vaughan, A. J. Urquhart, M. S. Tikhov, and R. M. Lambert, Surf. Sci., **578**, L85, 2005.

[86] G. Henkelman, B. P. Uberuage, and H. Jónsson, J. Chem. Phys., **113**, 9901, 2000.

[87] R. Manne and T. A. berg, Chem. Phys. Let., **7**, 282, 1970.

[88] J. Stöhr. Springer-Verlag Berlin Heidelberg, 1992.

[89] E. Frieden, Sci. Am., **227**, 52–60, 1972.

[90] G. Tu, V. Carravetta, O. Vahtras, and H. A. gren, J. Chem. Phys., **127**, 174110, 2007.

[91] L. Triguero, O. Plashkevych, L. G. M. Pettersson, and H. Ågren, J. Electron Spectrosc. Relat. Phenom., **104**, 195, 1999.

[92] B. Johansson and N. Mårtensson, Phys. Rev. B, **21**, 4427, 1980.

[93] A. Rosengren and B. Johansson, Phys. Rev. B, **23**, 3852, 1981.

[94] C. Göransson, W. Olovsson, and I. A. Abrikosov, Phys. Rev. B, **72**, 134203, 2005.

[95] W. Olovsson, I. A. Abrikosov, B. Johansson, A. Newton, R. J. Cole, and P. Weightman, Phys. Rev. Lett., **92**, 226406, 2004.

[96] W. Olovsson, , C. Gövsson, L. V. Pourovskii, B. Johansson, and I. A. Abrikosov, Phys. Rev. B, **72**, 064203, 2005.

[97] V. Feyer, O. Plekan, R. Richter, M. Coreno, K. C. Prince, and V. Carravetta, J. Phys. Chem. A, **112**, 7806, 2008.

[98] A. Stierle, C. Tieg, H. Dosch, V. Formoso, E. Lundgren, J. N. Anderson, L. Köhler, and G. Kresse, Surf. Sci., **529**, L263, 0000.

[99] B. Brena, Y. Luo, M. Nyberg, S. Carniato, K. Nilson, Y. Alfredsson, J. Åhlund, N. Mårtensson, H. Siegbahn, and C. Puglia, Phys. Rev. B, **70**, 195214, 2004.

[100] B. Brena, S. Carniato, and Y. Luo, J. Chem. Phys., **122**, 184316, 2005.

[101] B. Gao, Z. Y. Wu, and Y. Luo, J. Chem. Phys., **00**, 00.

[102] V. Feyer, O. Plekan, R. Richter, M. Coreno, K. C. Prince, and V. Carravetta, J. Phys. Chem. A, **112**, 7806–7815, 2008.

[103] J. Blomquist, L. E. Walle, P. Uvdal, A. Borg, and A. Sandell, J. Phys. Chem. C, **112**, 16616, 2008.

[104] H. Ågren, V. Carravetta, O. Vahtras, and L. G. M. Pettersson, Chem. Phys. Lett., **222**, 75, 1994.

[105] H. Ågren, V. Carravetta, O. Vahtras, and L. G. M. Pettersson, Chim. Acta., **97**, 14, 1997.

[106] V. Carravetta, O. Plashkevych, and H. Ågren, Chem. Phys., **263**, 231, 2001.

[107] M. Nyberg, Y. Luo, L. Triguero, L. G. M. Pettersson, and H. Ågren, Phys. Rev. B, **60**, 7956–7960, 1999.

[108] P. W. Langhoff. *Electron Molecule and Photon-Molecule Collisions*. Plenum, NY, 1979.

[109] P. W. Langhoff. *Theory and Application of Moment Methods in Many Fermion Systems*. Plenum, NY, 1980.

[110] N. Saliba, D. H. Parker, and B. E. Koel, Surf. Sci., **410**, 270, 1998.

[111] J. M. Gottfried, K. J. Schmidt, S. L. M. Schroeder, and K. Christmann, Surf. Sci., **511**, 65, 2002.

[112] W. X. Li, C. Stampfl, and M. Scheffler, Phys. Rev. B, **65**, 075407, 2002.

[113] A. Bogicevic and K. C. Hass, Surf. Sci. Lett., **506**, L237, 2002.

[114] S. M. McClure, T. S. Kim, J. D. Stiehl, P. L. Tanaka, and C. B. Mullins, J. Phys. Chem. B, **108**, 17952, 2004.

[115] T. S. Kim, J. L. Gong, and R. A. O. et al., J. Am. Chem. Soc., **128**, 6282, 2006.

[116] A. Vittadini, M. Casarin, and A. Selloni, Theor. Chem. Acc., **117**, 663, 2007.

[117] J. L. Gong, D. W. Flaherty, R. A. Ojifinni, J. M. White, and C. B. Mullins, J. Phy. Chem. C, **112**, 5501, 2008.

[118] J. L. Gong, D. W. Flaherty, T. Yan, and C. B. Mullins, ChemPhysChem, **9**, 2461, 2008.

[119] J. L. Gong, T. Yan, and C. B. Mullins, Chem. Commu., pages 761–763, 2009.

[120] D. L. Lahr and S. T. Ceyer, J. Am. Chem. Soc., **128**, 1800, 2006.